

AD-A176 969 DOCUMENTATION PAGE

1a. REPORT SECURITY CLASSIFICATION Unclassified		1b. RESTRICTIVE MARKINGS	
2a. SECURITY CLASSIFICATION AUTHORITY		3. DISTRIBUTION / AVAILABILITY OF REPORT Approved for public release; Distribution unlimited	
2b. DECLASSIFICATION / DOWNGRADING SCHEDULE		5. MONITORING ORGANIZATION REPORT NUMBER(S) AFOSR-TR- 87-0183	
4. PERFORMING ORGANIZATION REPORT NUMBER(S)		7a. NAME OF MONITORING ORGANIZATION AFOSR/NP	
6a. NAME OF PERFORMING ORGANIZATION Massachusetts Institute of Technology	6b. OFFICE SYMBOL (if applicable)	7b. ADDRESS (City, State, and ZIP Code) Building 410 Bolling AFB DC 20332-6448	
6c. ADDRESS (City, State, and ZIP Code) Building N10-201 155 Massachusetts Ave. Cambridge, MA 02139	8a. NAME OF FUNDING / SPONSORING ORGANIZATION Same as 7a	8b. OFFICE SYMBOL (if applicable) NP	9. PROCUREMENT INSTRUMENT IDENTIFICATION NUMBER AFOSR 84-0107
8c. ADDRESS (City, State, and ZIP Code) Same as 7b	10. SOURCE OF FUNDING NUMBERS		
	PROGRAM ELEMENT NO. 61102F	PROJECT NO. 2301	TASK NO. A7 WORK UNIT ACCESSION NO.
11. TITLE (Include Security Classification) (U) SPACE-CHARGE-INDUCED BREAKDOWN IN DIELECTRICS			
12. PERSONAL AUTHOR(S) Dr Chathan M. Cooke			
13a. TYPE OF REPORT FINAL	13b. TIME COVERED FROM 1 Jun 84 to 30 Sep 85	14. DATE OF REPORT (Year, Month, Day) 85 January 1986	15. PAGE COUNT 56
16. SUPPLEMENTARY NOTATION			
17. COSATI CODES		18. SUBJECT TERMS (Continue on reverse if necessary and identify by block number)	
FIELD	GROUP	Dielectrics, Optics, E-beam	
19. ABSTRACT (Continue on reverse if necessary and identify by block number) The work included experimental tests and theoretical modelling of space charge effects. The tests employed energetic electron beams as a means to inject controlled quantities of charge into test specimens. The use of electron beams is relevant to certain practical applications such as radiation effects and space craft charging, as well as being an important diagnostic tool for dielectric materials and for e-beam transport studies.			
20. DISTRIBUTION / AVAILABILITY OF ABSTRACT <input checked="" type="checkbox"/> UNCLASSIFIED/UNLIMITED <input type="checkbox"/> SAME AS RPT. <input type="checkbox"/> DTIC USERS		21. ABSTRACT SECURITY CLASSIFICATION Unclassified	
22a. NAME OF RESPONSIBLE INDIVIDUAL Major Bruce L. Smith		22b. TELEPHONE (Include Area Code) 202/767-4907	22c. OFFICE SYMBOL NP

DTIC FILE COPY

DTIC ELECTE
S FEB 24 1987 D

Shelf Copy
FINAL TECHNICAL REPORT

on

AFOSR-TR- 87-0183

SPACE - CHARGE - INDUCED BREAKDOWN IN DIELECTRICS

Contract/Grant No.: AFOSR-84-0107

for the

Air Force Office of Scientific Research

June 1, 1984 to September 30, 1985

Performed by:

Massachusetts Institute of Technology

Laboratory for Electromagnetic and Electronic Systems

High Voltage Research

Approved for public release;
distribution unlimited.

report prepared by:

Chathan M. Cooke,

Principle Investigator

Building N10-201

155 Massachusetts Ave.

Cambridge, MA 02139

Telephone: 617-253-2591

AIR FORCE OFFICE OF SCIENTIFIC RESEARCH (AFOSR)

NOTICE OF TECHNICAL INFORMATION TO DTIC

This technical report has been reviewed and is

approved for public release IAW AFR 19D-12.

Distribution is unlimited.

MATTHEW J. KETTER

Chief, Technical Information Division

- January 1986

87- 2 20 178

SPACE-CHARGE-INDUCED BREAKDOWN IN DIELECTRICS

Table of Contents

	<u>Page</u>
1. Project Overview	1
2. Introduction	1
2.1 Space Charge Effects	1
2.2 Basic Breakdown Processes	2
2.3 Dielectric Materials	3
2.4 Experimental Methods	3
2.5 New Diagnostics	5
3. Characteristics of Space-Charged-Induced Breakdown	5
3.1 Branched Breakdown Morphology	5
3.1.1 Breakdown channel position	5
3.1.2 Breakdown channel size and extent	8
3.1.3 Relation to fractals	8
3.2 Processes During Channeling	11
3.2.1 Integrated emitted light	11
3.2.2 Currents during channeling	16
3.2.3 Local charge density variation	16
3.2.4 Velocity of propagation	23
3.2.5 Transferred charges	23
3.2.6 Incident flux rate effects	27
3.3 Material Effects	27
3.3.1 Initiation, channel propagation	27
3.4 Embedments	31
3.4.1 Spheres	31
4. Model for Charging of Dielectrics by E-Beam Irradiation	31
4.1 Internal Charge Decay	31
4.1.1 Decay with time, initial charge effects	31
4.1.2 Temperature effects and decay	31
4.1.3 Mobility model	35
4.2 Initial Net Internal Volume Charge	36
4.3 Position of Charge Layer	36

<input checked="" type="checkbox"/> <input type="checkbox"/> <input type="checkbox"/>

Availability Codes	
Dist	Avail and/or Special
A-1	



	<u>Page</u>
5. Model for Breakdown Through Volume Space-Charged Regions	38
5.1 Propagation Model	38
5.1.1 Absolute available energy	38
5.1.2 Relative available energy, Channel impedance effects	43
5.2 Proposed Model for Charge Injection and Breakdown without E-Beam	44
6. New Diagnostics	46
6.1 Electro-optic Measurements of E-Beam Implanted Charges	46
6.2 Electro-acoustic Method	46
7. Conclusions	52
8. Acknowledgements	52
9. References	52

SPACE - CHARGE - INDUCED BREAKDOWN IN DIELECTRICS

Massachusetts Institute of Technology
Laboratory for Electromagnetic and Electronic Systems
High Voltage Research

1. PROJECT OVERVIEW

This report describes the results of a 15 month study, sponsored by AFOSR, Directorate of Physical and Geophysical Sciences, concerning dielectrics and more particularly the influence of accumulated space charges on dielectric breakdown. The work includes experimental tests and theoretical modelling of space charge effects. The tests employed energetic electron beams as a means to inject controlled quantities of charge into test specimens. The use of electron beams is relevant to certain practical applications such as radiation effects and space craft charging, as well as being an important diagnostic tool for dielectric materials and for e-beam transport studies.

The investigations were organized into 5 study tasks: discharge extent, charge transfer, channeling location, flux rate effects, and a propagation model. The results from these tasks cover many important issues, which for purposes of this report have been grouped into the broad categories of measured characteristics and models. Specifically, the report includes, after the introduction (2), sections on the characteristics of induced breakdown (3), modelling of the charging process (4), modelling for breakdown within a charged volume (5), new diagnostic methods (6) and conclusions (7).

2. INTRODUCTION

2.1 Space Charge Effects

Dielectrics by definition impede the flow of electric charges and hence can act to store electric charges on their surface or in their volume and thereby cause major changes in electric field distributions. The residence time for such stored charge varies from material to material, with the type of carrier, and according to the type of transport process. When the accumulated space charge is large, it can produce electric fields which can exceed those which the dielectric can sustain and breakdown can occur.

Situations where space charges are often important include a range of different applications and can be separated into cases with and without e-beams. When e-beams are not present, space charges can still accumulate but by other charge transport processes.

Example applications include:

With e-beams:

- basic beam interaction physics
- dosimetry
- radiation damage
- multichannel switching
- accelerator technology

Without e-beams:

- electrical treeing
- aging, degradation
- reliability
- surface flashover
- solid dielectric interfaces

Models to describe the charge accumulation stage are usually based upon the continuity equation which is coupled to Poisson's equation for the electric field. A driving term which accounts for charge injection, such as from an e-beam is needed to activate the process. These equations are:

$$\nabla \cdot \bar{J} + \frac{\partial \rho}{\partial t} = 0$$

$$\bar{J} = \sigma \bar{E} + \rho \mu \bar{E} + \bar{J}_0$$

$$\nabla \cdot \bar{E} = \rho / \epsilon, \quad \int \bar{E} \cdot d\mathbf{l} = -V$$

where J is the current density, ρ the net charge density, σ the material conductivity, E the local electric field, μ the carrier mobility, J_0 the current density due to external generation sources, and ϵ the dielectric permittivity.

2.2 Basic Breakdown Processes

When space charge generated fields are high and breakdown occurs it is a sudden irreversible event with channels which rapidly develop and propagate through the dielectric. Space charge induced breakdown has some characteristics which are in common to those of usual applied voltage breakdown and in addition some characteristics which are unique. As developed in this study space charge effects were isolated by not using an electrode pair to apply an electric field to the dielectric. Without an externally applied field, only the accumulated space charges held by the dielectric produced the electric fields and hence space charge effects could be clearly isolated for study. The conditions associated with charge accumulation, channel initiation and channel propagation were of interest in this work.

Models for the breakdown process are less developed than those for the charge accumulation stage. However, by use of controlled distributions of implanted charges as employed in this work, it has been possible to determine major parameters of importance to the breakdown process.

2.3 Dielectric Materials

The role of the dielectric material on space charge induced breakdown involves three main processes:

- accumulation
- breakdown inception
- breakdown extent, treeing.

Firstly, the material influences the net charge accumulation by its inherent charge transport and conduction processes. Second, once charge has accumulated, basic material insulation strength and local defects influence the initiation of breakdown channels. And thirdly, channel propagation is influenced by chemical and plasma details including, power loss rates, plasma waves, and conductivities in the channel. In these investigations many of the tests were made with polymethylmethacrylate (PMMA) since it readily accumulated charges and is transparent for optical analysis. Other materials included polycarbonate, epoxy and Mylar.

2.4 Experimental Methods

These studies have employed an unusual procedure for insulation studies, the direct deposition, ie. implantation, of charges within the test dielectrics. Macroscopic volumes of space-charge were implanted within the solid dielectric samples by means of an energetic electron beam. To do this a Van de Graaff accelerator with controlled beam energies up to 3 MeV was used. These energies cause charge penetration to centimeter depths in the test materials and under certain conditions lead to tree channel breakdown paths. Advantages of this method include:

- i) control of amount and spatial distribution of charge
- ii) direct measurement of currents during propagation
- iii) direct measurement of channel formation velocities
- iv) measurement of channel morphology
- v) production of extended channels for comparison to models

The typical procedure for implanting charge in the test specimens by means of an electron beam has been described in detail in reference [1]. These studies employed the same basic methods with a beam of several microamperes usually directed at the broad face of a sample for a time sufficient to accumulate a net charge on the order of $1 \mu\text{C}/\text{cm}^2$, Figure 1. The magnitude and spatial distribution were controlled by a combination of beam intensity and by masking. Discharges could then be initiated from various locations, for example from one end as in Figure 2.

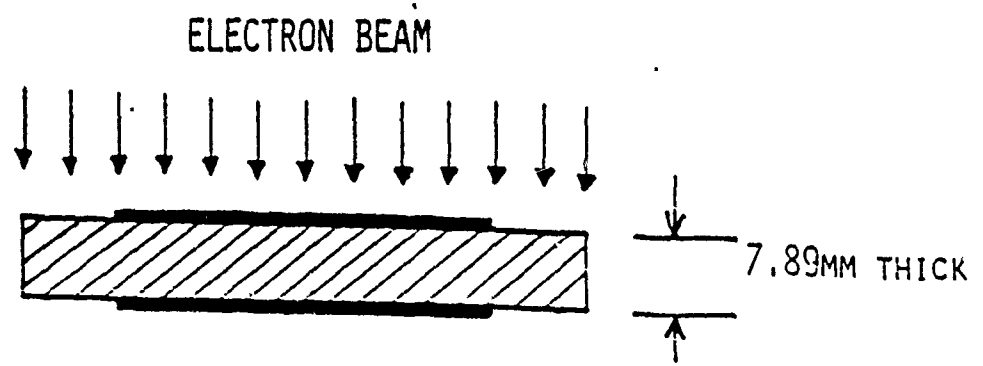


FIGURE 1. SAMPLE GEOMETRY, 5CM X 5CM WIDTH, 30MM DIA. METALLIZATION

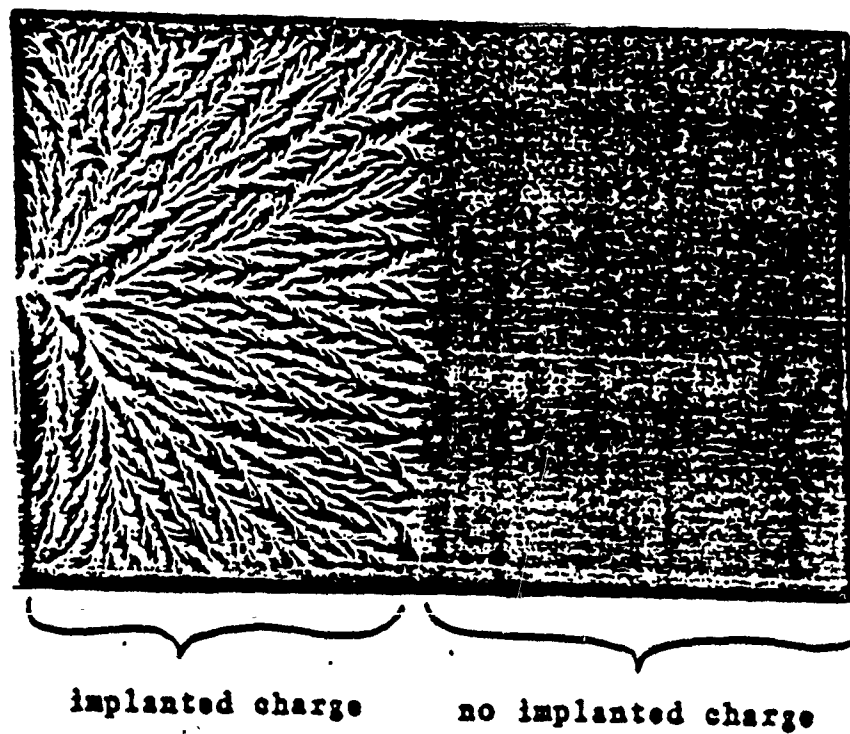


Figure 2 Electrical "tree" discharge stops propagation at implanted charge boundary

MIT-HUKL

2.5 New Diagnostics

In order to better determine the actual distribution of accumulated charges prior to breakdown it was necessary to employ new diagnostic methods. While published articles had indicated charge accumulation by dosimetry and collected current methods [2,3], there was a lack of hard evidence for true charge distributions created by e-beam irradiation without inserted probe electrodes. To more directly measure the charges, two non-destructive methods were used; one used the Kerr electro-optic effect and the other a newly developed electro-acoustic technique. Both were successful and are described further in Section 6.

3. CHARACTERISTICS OF SPACE-CHARGE-INDUCED BREAKDOWN

In this section the attributes of space charge induced breakdown are detailed. The branched breakdown morphology, its depth in the dielectric, and the channel sizes and lengths are presented. Then events during channel development are discussed, such as: emitted light, currents and collected charge. Finally, material specific differences are discussed.

3.1 Branched Breakdown Morphology

The dielectric breakdown induced by accumulated space charges has, in every case, lead to a breakdown path which was an extended branched structure. A permanent damage path composed of a tree-like set of interconnected channels is produced, Figure 2. These channels do not recross the same region or reconnect one another to form loops. An exception occurs when there has been multiple charge and discharge events one after the other with repeated charge implantation into the same volume.

3.1.1 Breakdown channel position

Except for a single exit path to the surface, the physical location of the breakdown channels resulting from e-beam implanted charges was normally within the dielectric and mainly within the region of highest space charge density. The location of the channel exit point and the breakdown initiation was often stimulated by a point electrode pushed into the surface of a charged sample, as illustrated in Figure 3. The depth below the dielectric surface where the channelling occurred was reasonably confined and determined by the energy of the electron beam. Figure 4 shows typical channel depth values vs e-beam energy. In addition, for comparison, expected electron range values [1] are also shown. Note that the channels are typically at a depth about half that for the range. This means that on average the net electronic charge accumulates at about the half range position in charge storing dielectrics. This is in general agreement with the published findings of Gross and Wright [2] and of the electro-acoustic results, Section 4.

AFTER IRRADIATION
SIDE VIEW - DISCHARGE

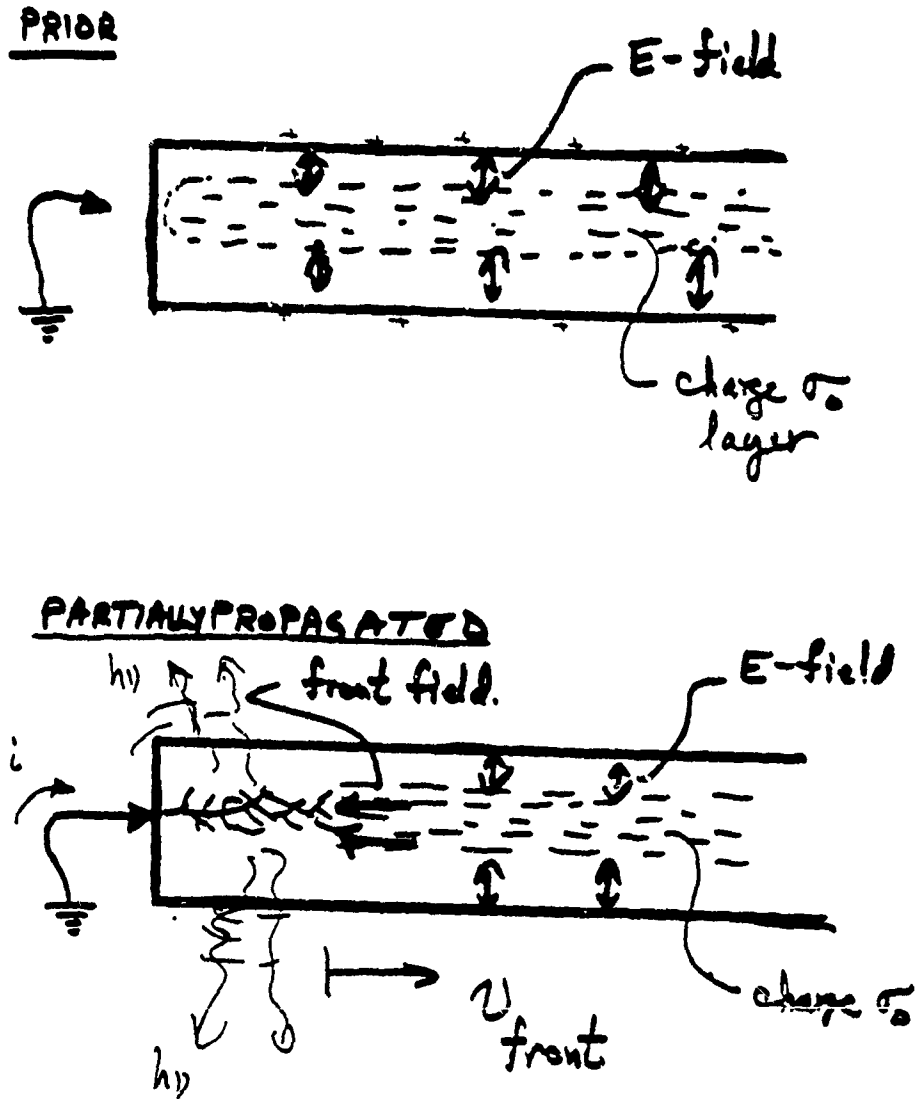
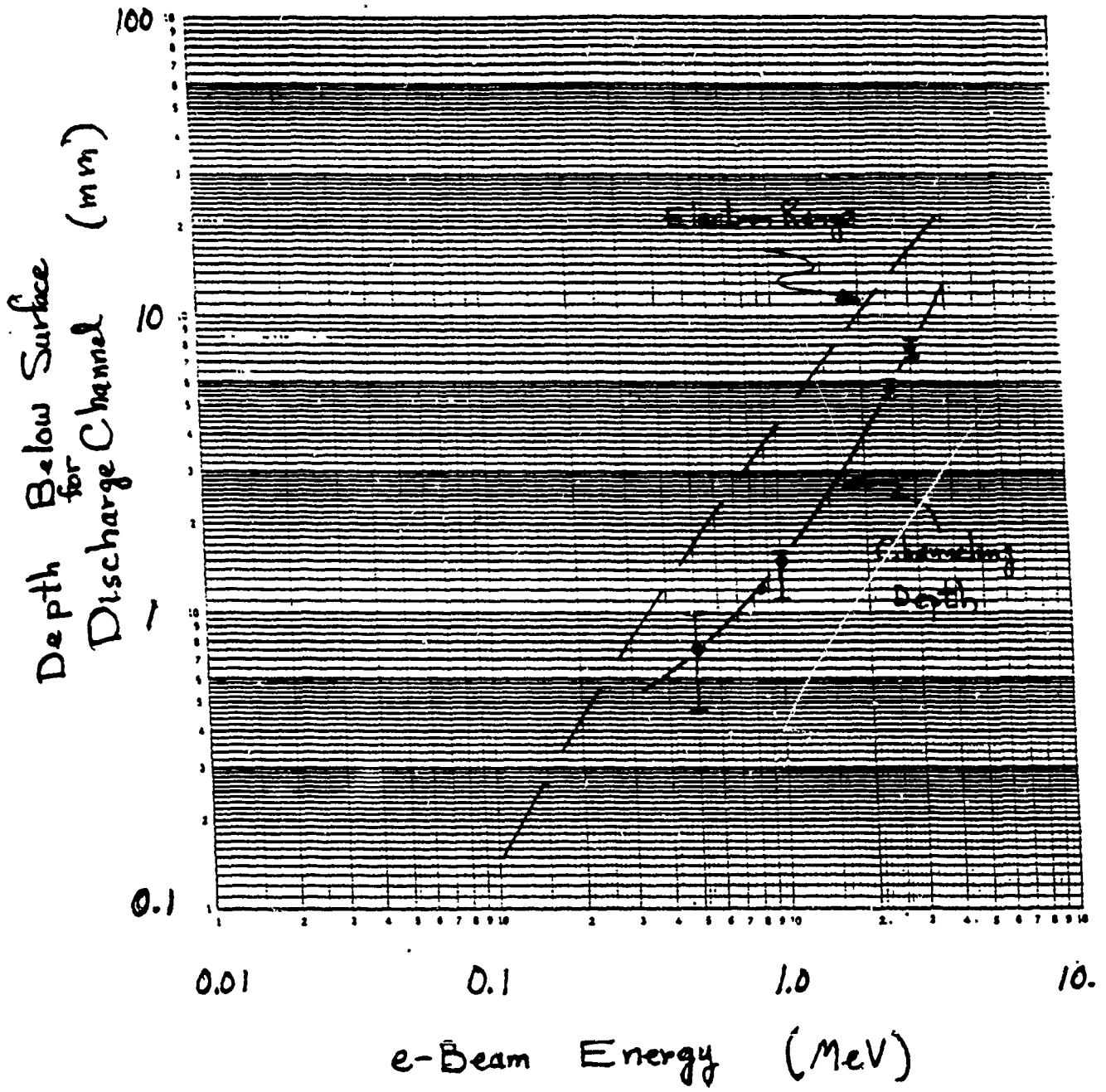


Figure 3 Schematic view of breakdown initiation and propagation

MIT-HURL



MIT-HVRL

Figure 4 Channeling Position

3.1.2 Breakdown channel size and extent

The breakdown channels were found to propagate to a self-stopping distance which depended upon the space charge density in the material. While an earlier study had shown the propagation length increased with electron irradiation dose [1], in this work the role of the charge density was more explicitly identified. In particular, the charge density was changed in one set of samples by means of cooling the samples to dry ice temperature, -78°C . The cold samples had greatly reduced charge mobilities so that for a given incident charge, the cold samples contained more accumulated charge and as a result exhibited longer channel propagation. This difference is shown in the data of Figure 5.

The greater charge density sustained in the cold samples was quantified by means of the electro-acoustic charge measurement method, as described in Section 4 concerning charge accumulation. Samples of PMMA were measured for total stored charge when they were held at various temperatures. The charge content vs time for these cases showed that at room temperature a significant amount of charge was already transferred out of the sample within a few minutes from e-beam injection. This time corresponds to the amount of time needed to perform the propagation length test. The amount of charge loss is about 25% which accounts for the reduced propagation length at room temperature shown in Figure 5.

For the case of polycarbonate material the results were different. In a manner similar to PMMA a minimum accumulated charge was needed to initiate breakdown channels in polycarbonate. But once started, they propagated for very long distances, even 1/2 meter, at moderate charge densities. The difference appears to be the result of a significantly lower channel impedance caused by carbonization. Other parameters, such as currents and velocities were not so different between PMMA and polycarbonate as will be discussed later. The role of the channel impedance is discussed in the section on modelling, Section 5.

The length of the discharge was also found to depend slightly on the width of the charged region. This effect is shown in Figure 6. Note that once a sample was 4 to 5 cm wide there was little difference from that for a much wider sample of 10 cm or so. The reduction for narrow widths appears to be another example of how reduced internal fields reduce the channel propagation.

3.1.3 Relation to fractals

The visible branched structure of the breakdown channels looks much like a tree or an aerial view of drainage erosion patterns. These structures have been analyzed in mathematical form by means of a formalism called fractals as developed by Mandelbrot. [4] For the case of space charge breakdown patterns, three regions were analyzed. One was the extreme end region

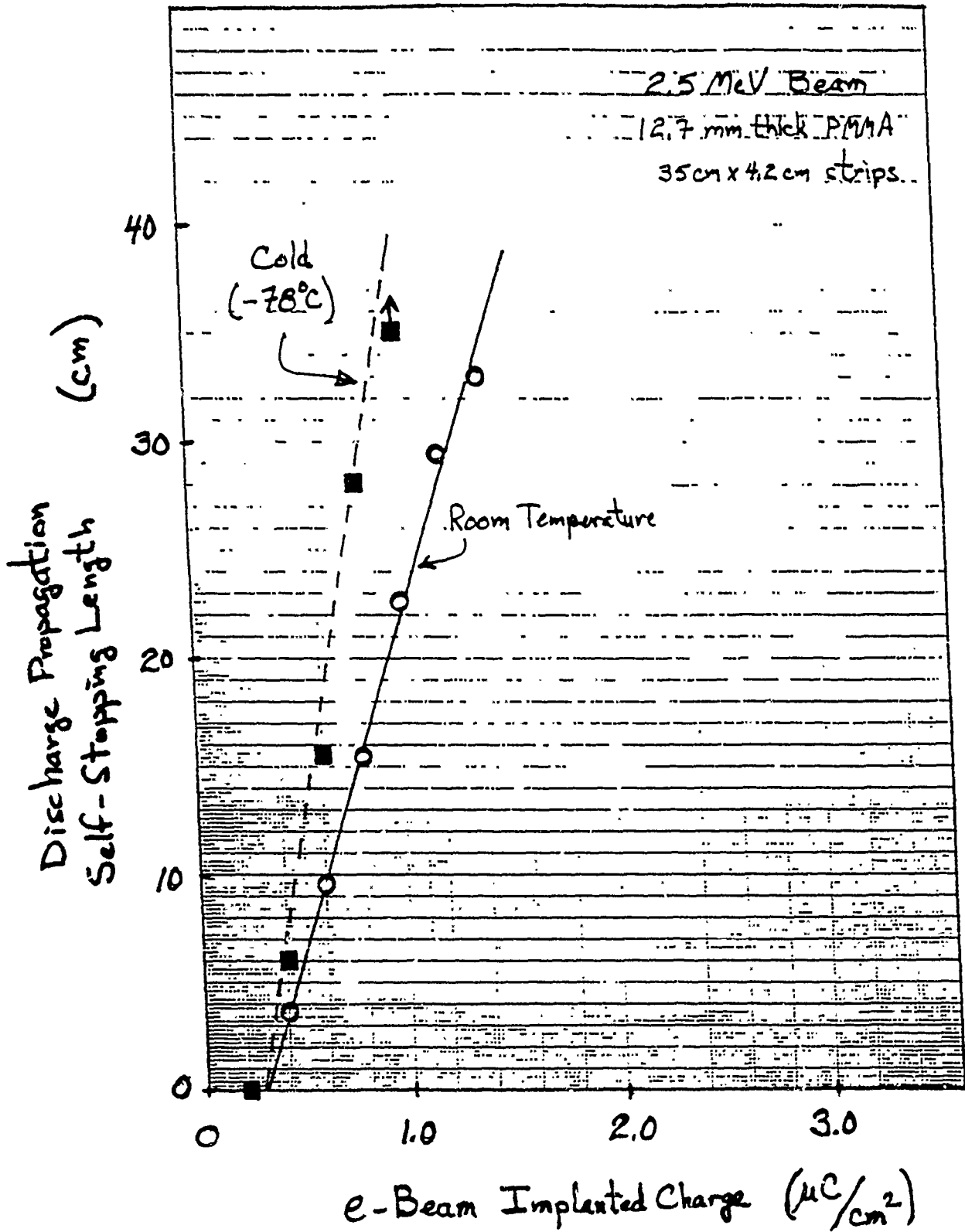


Figure 5 Self-Stopping Length in PMMA

MIT-HVRL

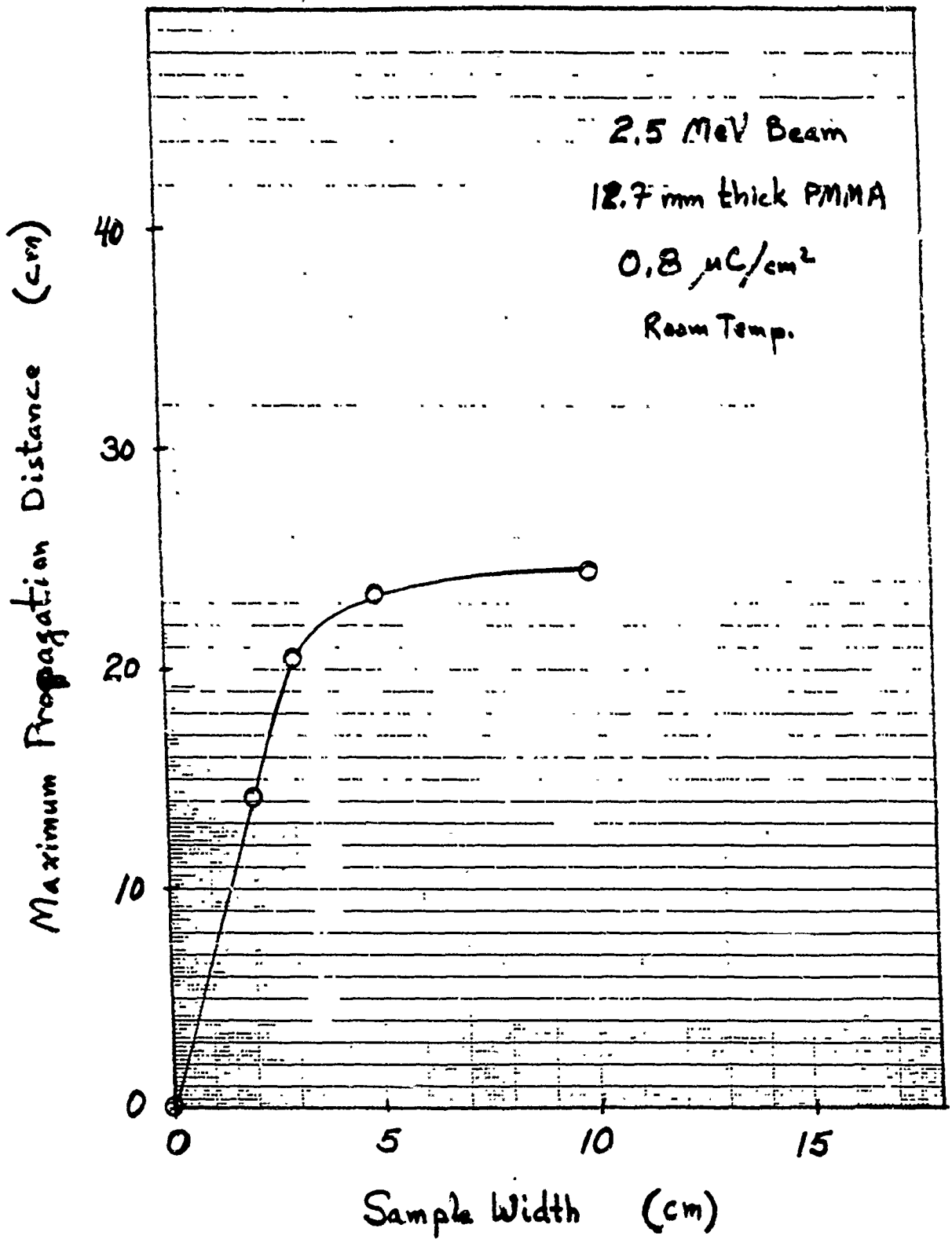


Figure 6 Sample Width Effect

where the channels stopped propagation even though additional space charge was present, Section 3.1.2, the next region was in the central portion and the third near the discharge root.

A quantity called the 'branching order' is used to determine the pattern of the branching process. For the case of the tip region, an expanded view of the channel structure is shown in Figure 7. The measured branching order vs position is shown in Figure 8. The near constant slope indicates that the branching process is a regular event.

According to fractal theory the negative slope corresponds to the system dimension. One implication is that similar dimensions correspond to systems which operate under the same basic physical principal, in this case that energy loss is minimized. The conclusion is that the fractal interpretation lends support to the model that the branched breakdown structure, is a regular pattern which may involve an energy minimization.

3.2 Processes During Channeling

In this section the characteristics of events which occur during the branched channel propagation are presented. Light emission, electric currents, charge transfer, and the role of local variations in charge density are topics that are presented.

3.2.1 Integrated emitted light

To help establish the characteristics of the channeling processes the integrated emitted light produced by the channeling was recorded and compared to the physical damage caused by the channeling. Specifically, open shutter photographs of several PMMA samples were taken during the channel development. These emitted light images were then compared to subsequent images of the physical damage. Figures 9 and 10 show two cases of emitted light and physical damage. There is very good correlation between the two. The unusual path of the discharge pattern in Figure 10 was made by masking a portion of the sample with two lead disks so that the space charge was excluded from these two circular regions.

The current and light brightness appear to be quantitatively correlated so that emitted light may be used as a good diagnostic for discharge damage. Generally, it can be seen from the figures that the brighter regions correspond to the 'trunk' channels where larger currents of longer duration are anticipated. To quantify this, induction pickup current detectors at different locations along a sample should be compared to the emitted light in the corresponding regions. Such tests were beyond the scope of this program.

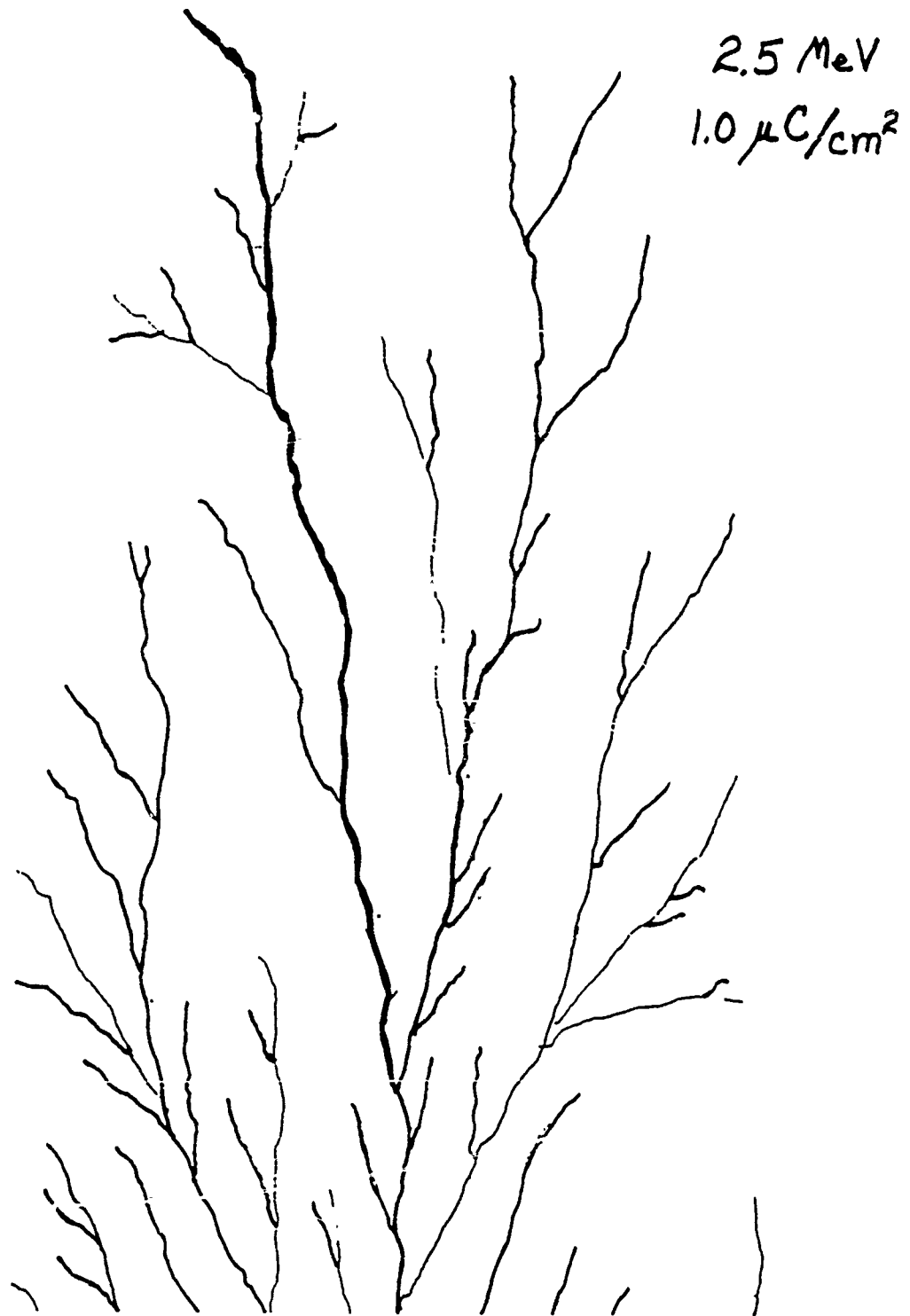


Figure 7 Tip Region, Expanded View of Self-Stopping Discharge

MIT-HVRL

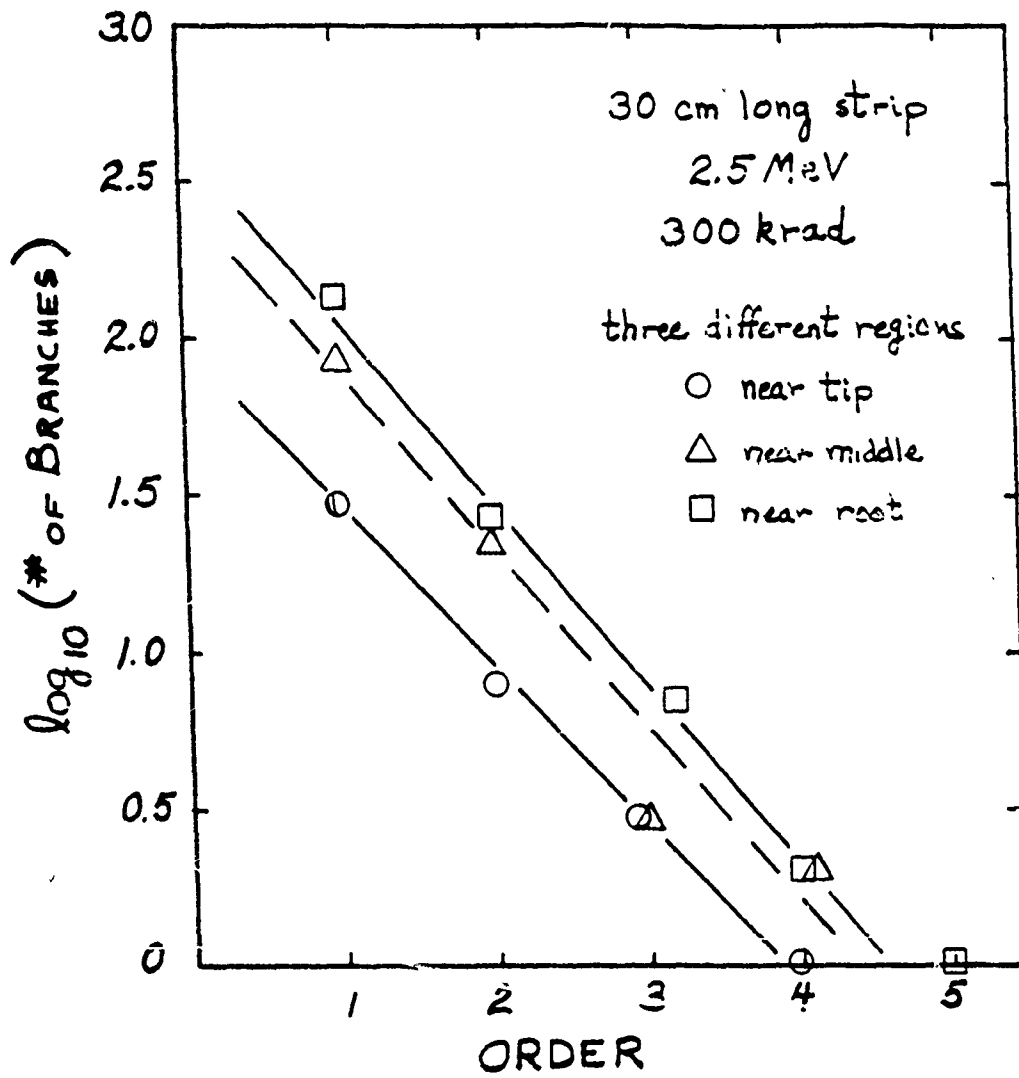
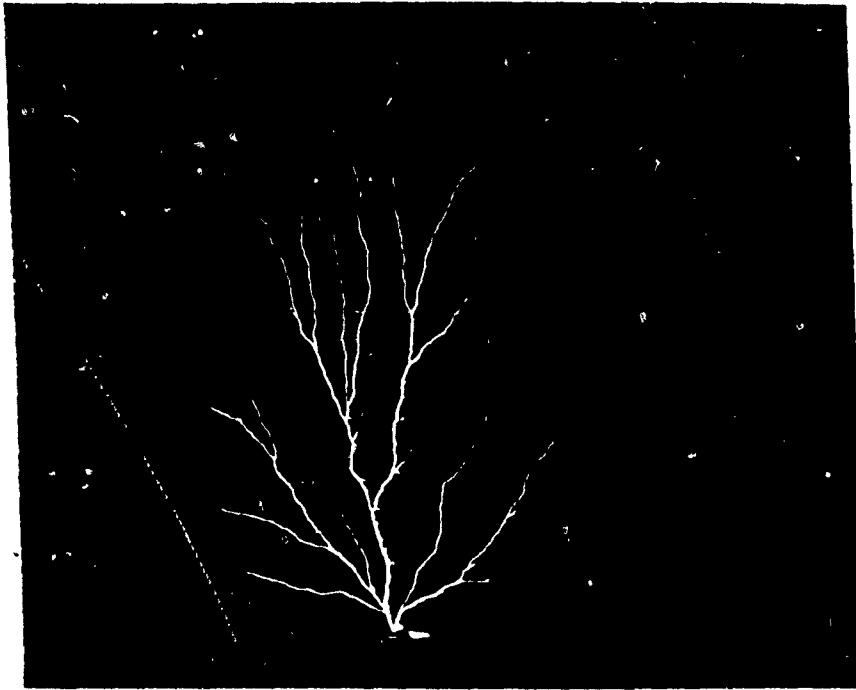


Figure 8 Branching Analysis



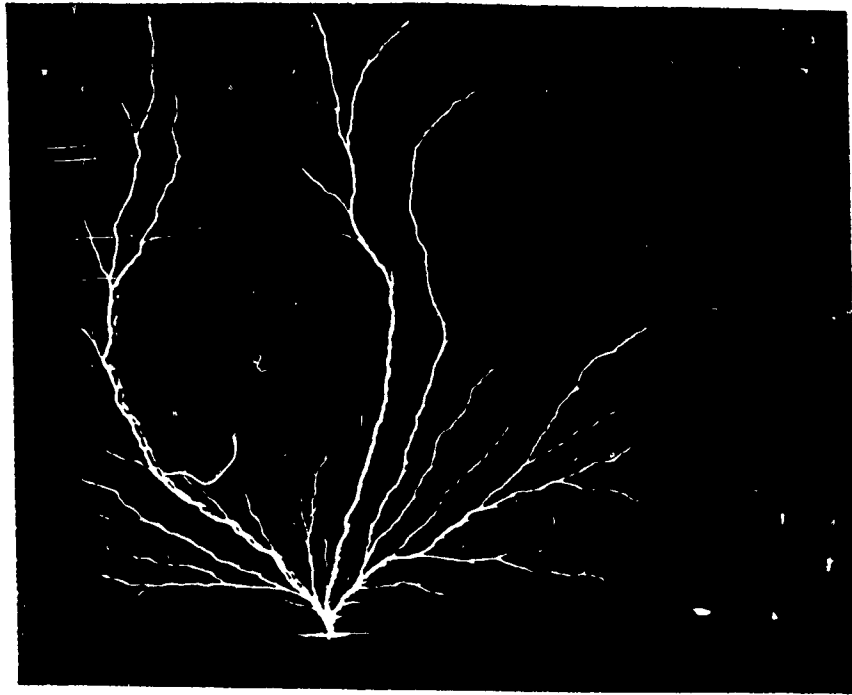
(a) Open shutter emitted light



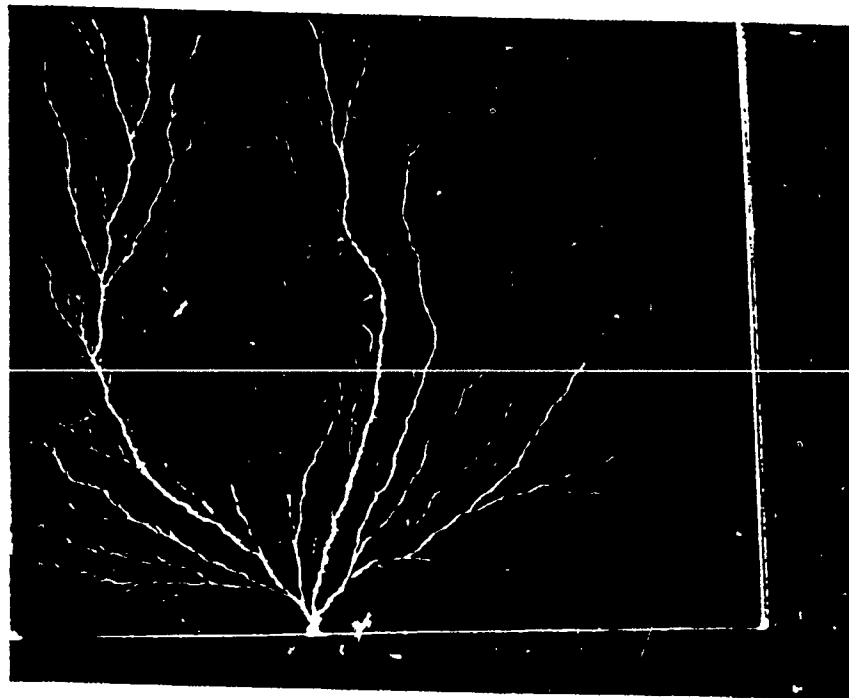
(b) Damage Channeling

Figure 9 Channeling Process, Uniform Charge

MIT-4UPL



(a) Open shutter emitted light



(b) Damage Channeling

Figure 10 Channeling Process, Non-uniform Charge

MIT-HVRL

3.2.2 Currents during channeling

The total current during space charge induced breakdown events was recorded and showed a remarkable correlation to channel development. The current through the main channel and out the 'exit' path was measured by means of a fast pulse Rogowski coil (10 ns risetime) around a short length conductor attached to the exit path (root) region. A strip-line geometry was used to keep fast time, nanosecond, resolution. Typical currents were in the range of 10 to 100 amperes and lasted for about 200 to 800 ns. For a uniform implanted charge density, the current immediately rose to a peak and slowly decayed during the propagation, Figure 11. The decay of current corresponded to increased channel length.

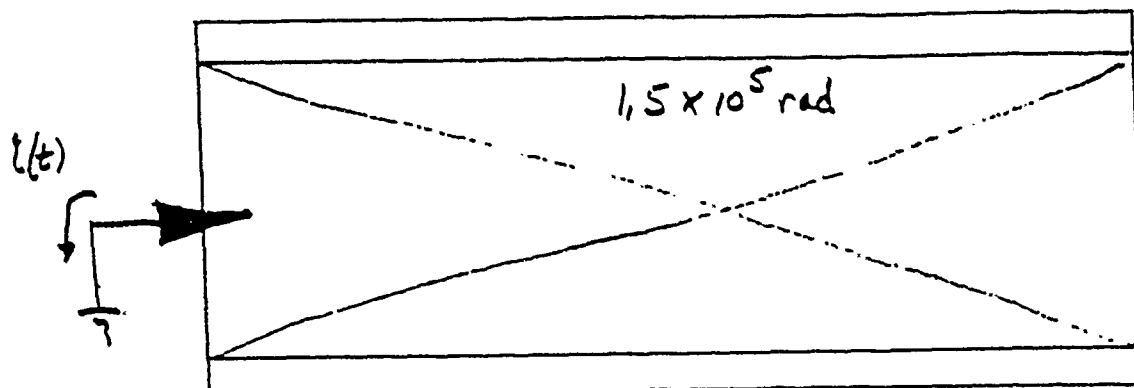
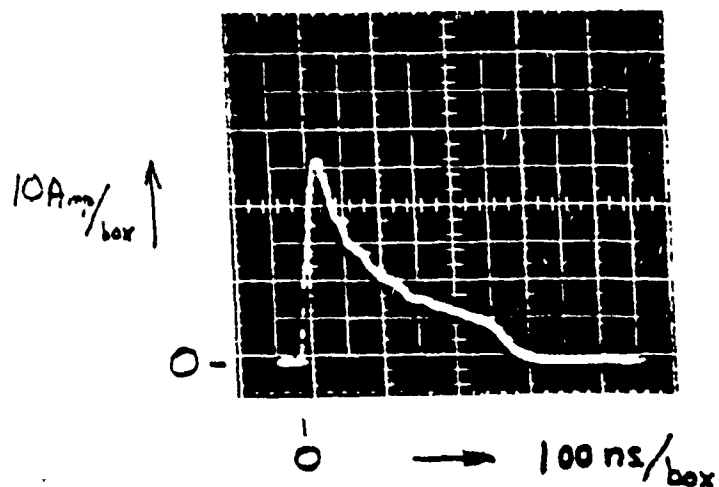
3.2.3 Local charge density variation

More importantly, the current waveforms were very consistent with the local charge density. Thus, when the implanted charge was enhanced or reduced in a local region, the change was observed as a corresponding change in the current waveform at the channel base, ie. root, when the discharge tip passed through the region of different charge density. The synchronism of increase and decrease in current with a pattern of high and low charge density regions respectively was very strong, Figures 12 and 13. Because of the rapid response in root current, even down to 10 ns, it appears that the change in discharge intensity according to tip region conditions is evident along the whole length of channel connecting to that region. The strong control of discharge propagation by local charge variations was clearly established in a series of five types of measurements:

- a) step increase, Figure 12
- b) 4 step ladder, Figure 13
- c) gap jumping, Figure 14
- d) reservoir, Figure 15
- e) steering, Figure 16.

The first two (a & b) show current jumps in accordance with an oscillating in space distribution of volume space charges. The next (c) shows the strong reduction in current as the propagation penetrates a short region of no charge. The sudden jump increase in current when a discharge propagates into a reservoir of charge is demonstrated in case d). And finally, the path of propagation (e) is shown to accurately follow a meander path of implanted charge.

Overall, there is very consistent evidence that the local charge density determines the intensity, direction, and (as is shown in the next section) the velocity of the channel propagation. This finding is consistent with an available energy model for channel development as discussed in Section 5.



PMMA Sample, 12.7 mm thick

Figure 11 Channel propagated full length of 14 cm in about a time of 500 ns according to the total collected current waveform

MIT-HURL

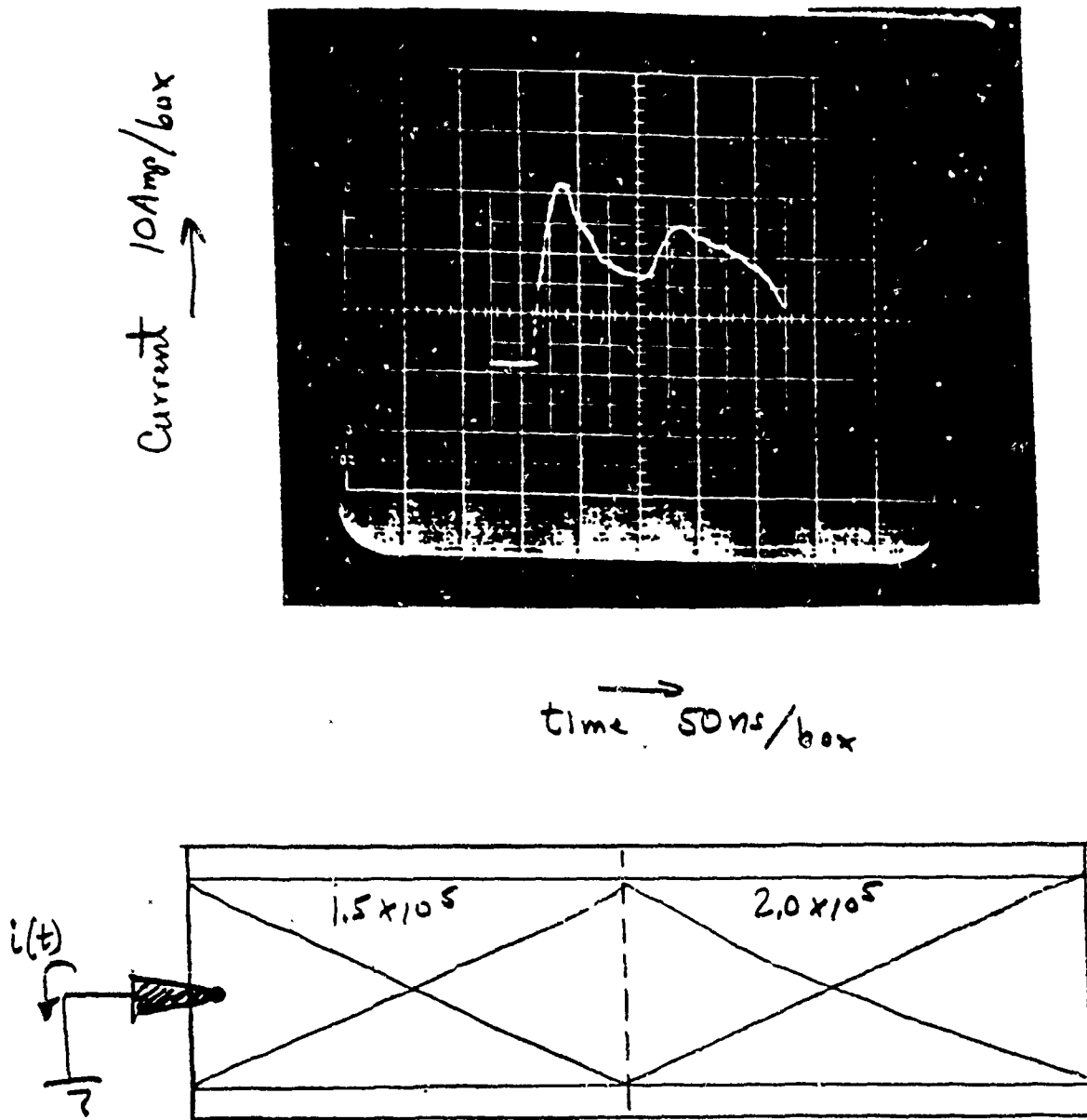


Figure 12 Rohm and Haas PMMA, Cold
Step increase implanted charge

MIT - HVRL

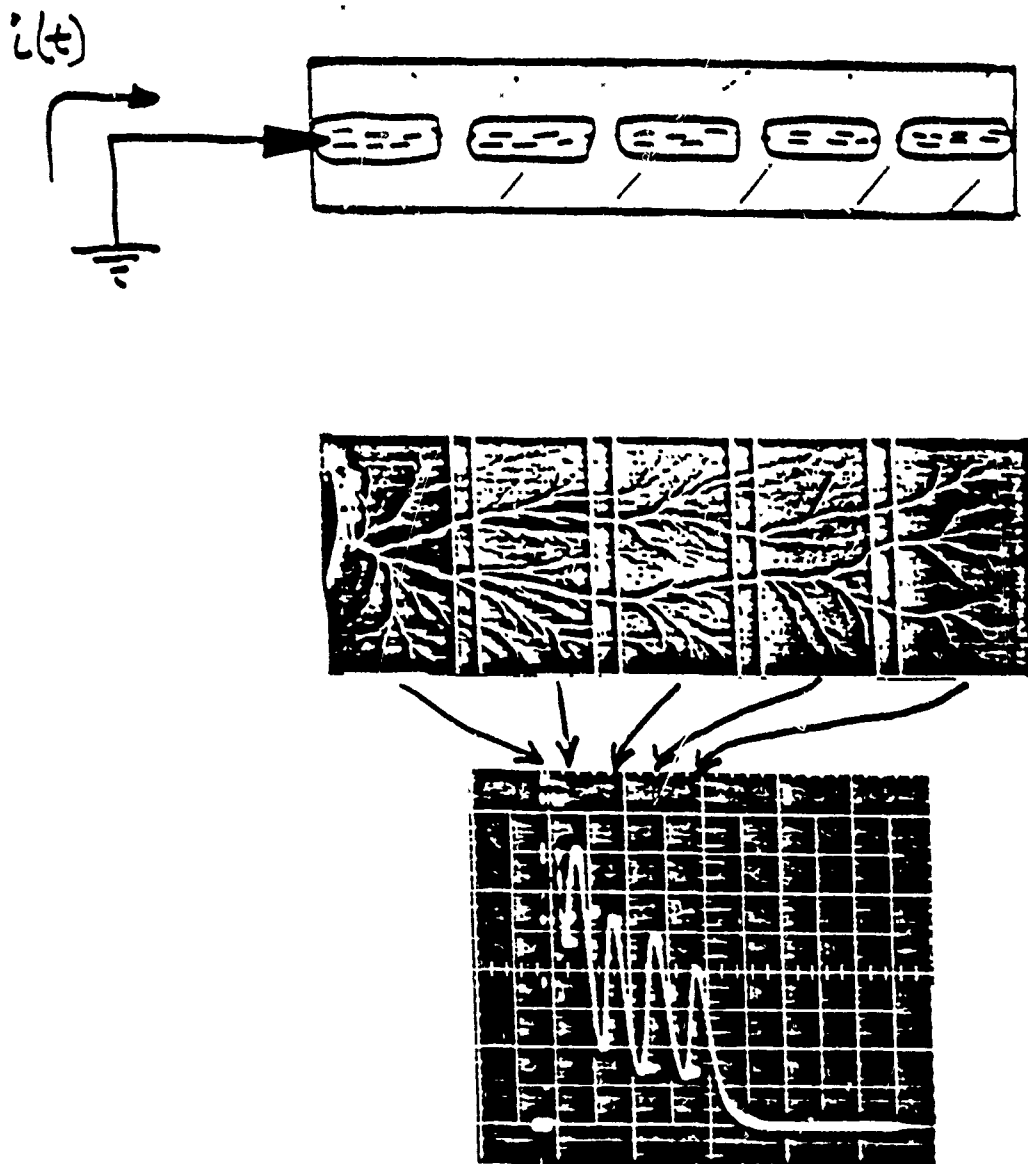


Figure 13 Discharge pattern and discharge current from non-uniformly charged PMMA, alternating₂ segments with 25 mm length at $0.8 \mu\text{C}/\text{cm}^2$ and 5 mm length at 0 charge, vertical at 10 Amp/box, horizontal at 100 ns/box

MIT-HVRL

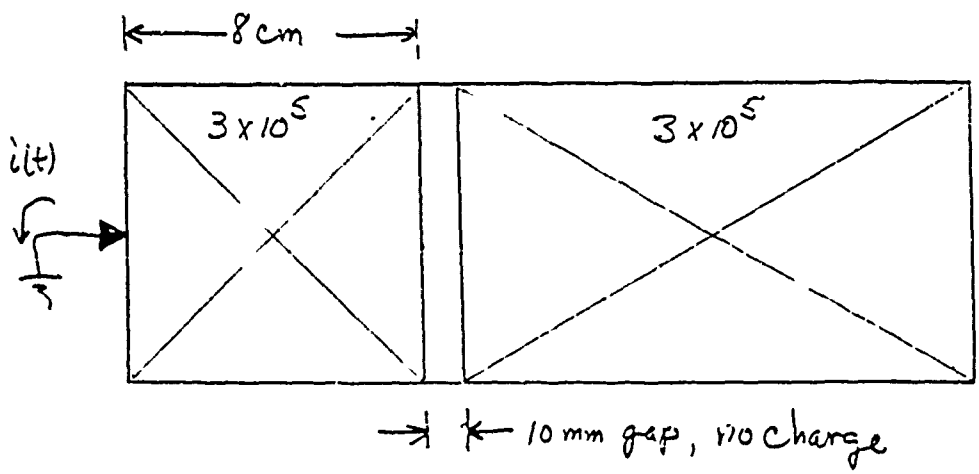
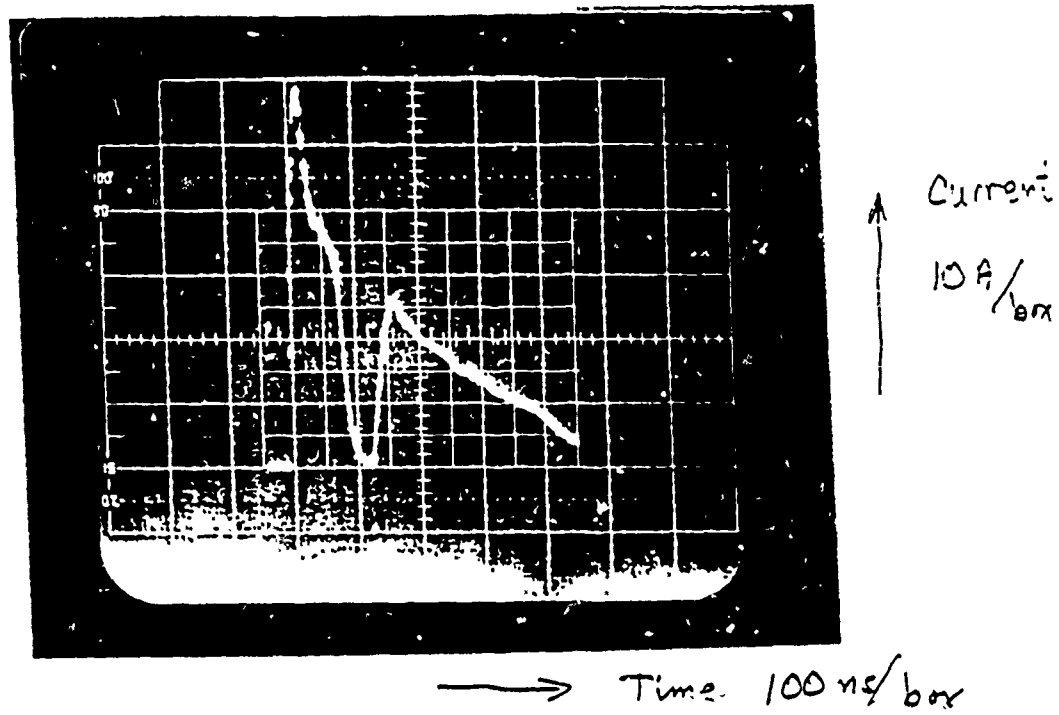


Figure 14 Gap jumping by propagating channel

MIT-HURL

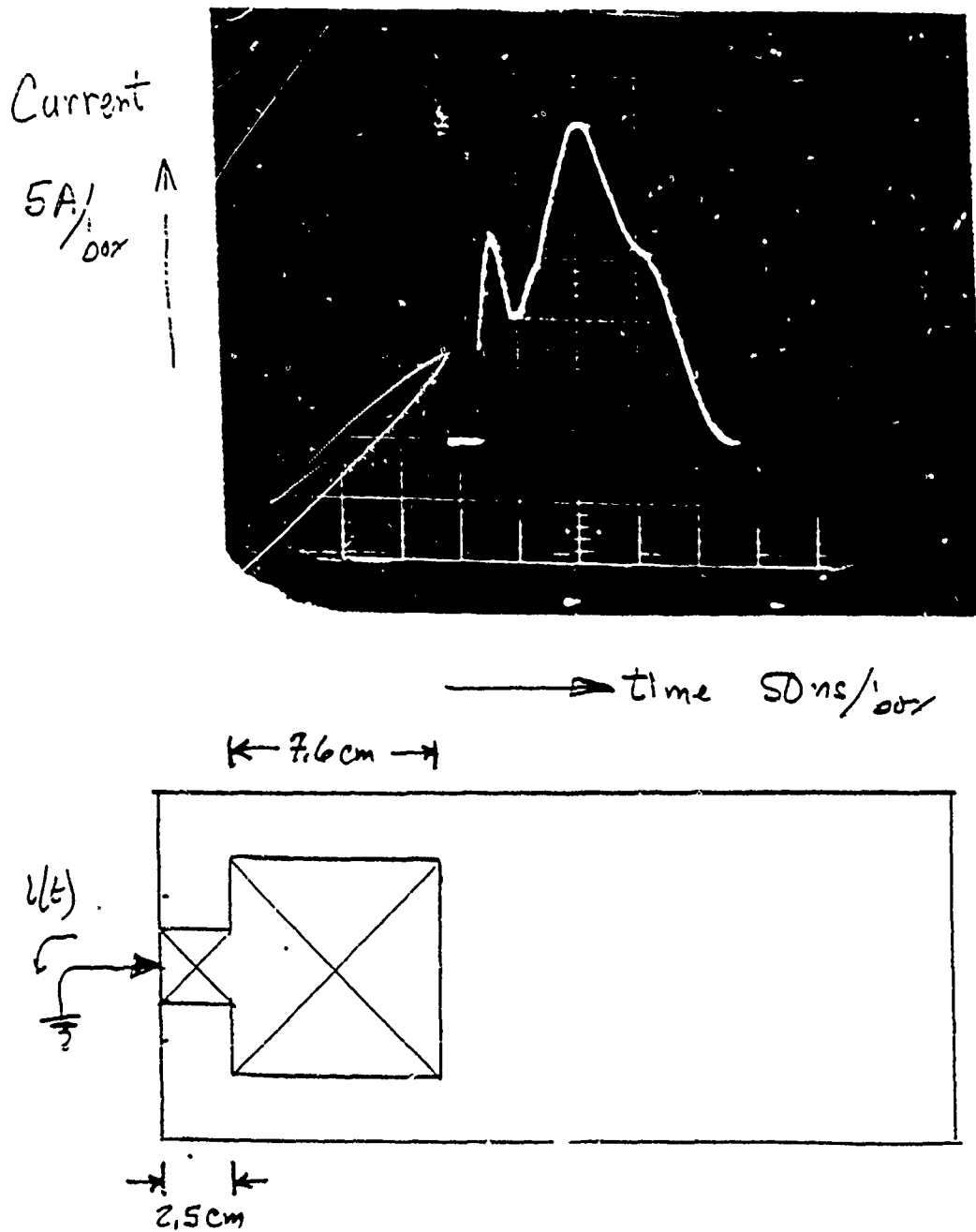


Figure 15 Charge Reservoir

MIT-HURL

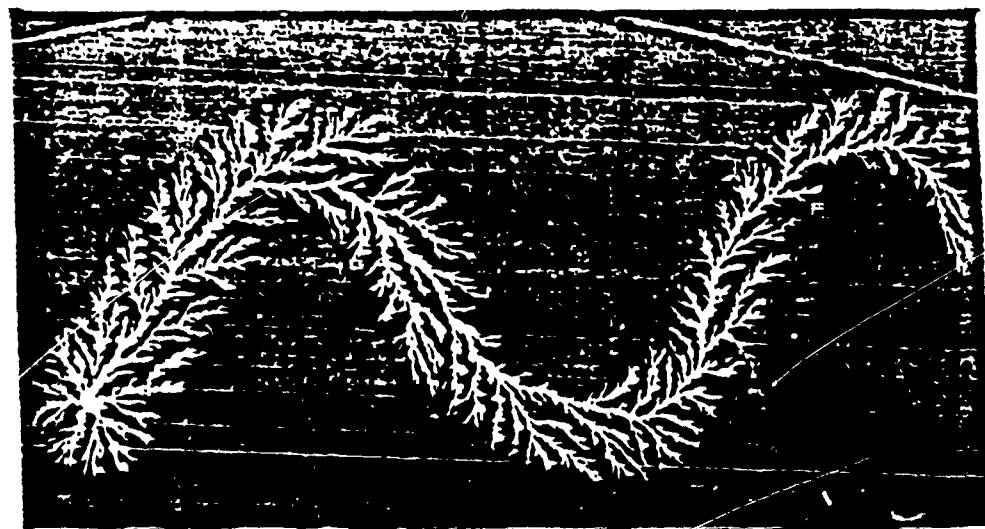


Figure 16 Electrical tree follows contour of
implanted charge

MIT-HVRL

3.2.4 Velocity of propagation

The velocity of propagation of the channeling discharge was measured by means of a relative technique which compares the simultaneous discharges in two adjacent paths, the so-called interferometer method. [1] The results indicate that the velocity increases as about the square of the charge density. These tests were made with cooled samples so as to avoid the problem of charge leakage during setup. Note that Polycarbonate and PMMA exhibit similar results, Figure 17.

A second method to determine velocity is by means of the 'ladder' pattern of Figures 13. Because the charge spacing is at equal intervals, the time between current peaks is inversely proportional to velocity. This assumes that the current change at the root, where the current monitor is located, does not have a delay which varies appreciable with the length of the channel. The figures indicate that the velocity is relatively constant with channel length and is about 10^5 cm/sec, although it does slow down somewhat for extended lengths.

3.2.5 Transferred charges

In addition to tests with a current monitor to measure the total current to the root of the discharge, some tests were made with a 10 μ fd capacitor in series with the lead so as to measure the net charge transferred by the channeling discharge in PMMA. The results of these tests are given in Figure 18. For a fixed level of implanted charge density the amount of charge transferred is relatively high for short samples and becomes progressively lower for longer samples. Note that this data uses an implanted stored charge value of $0.34 \mu\text{C}/\text{cm}^2$ or about 28% of the incident beam for the irradiation level of 3 kGys used on these samples.

The reduction in charge transfer efficiency with increased propagation length is expected from the fact that the channeling reaches the limit of its extent while at the same time maintaining a substantial velocity until it suddenly stops. That is, the channeling appears to be less effective in gathering energy and hence charge at extended distances. The reduced charge collection is also consistent with the reduced current as channels become long. The conclusion is that a substantial portion of net charge remains in the sample in regions where long channels propagate, and the efficiency of obtaining electrostatic energy from the space charge is reduced by long channels in PMMA.

The charge collection efficiency for fixed size disk samples of 46 cm^2 irradiated active area was measured vs the total electron injection. The results are shown in Figure 19. Note that some of the reduction in the fraction of charge collected at higher injected charge levels is the result of less fractional stored charge at the moment of measurement, see sections 3.2.6 and 4.1.2.

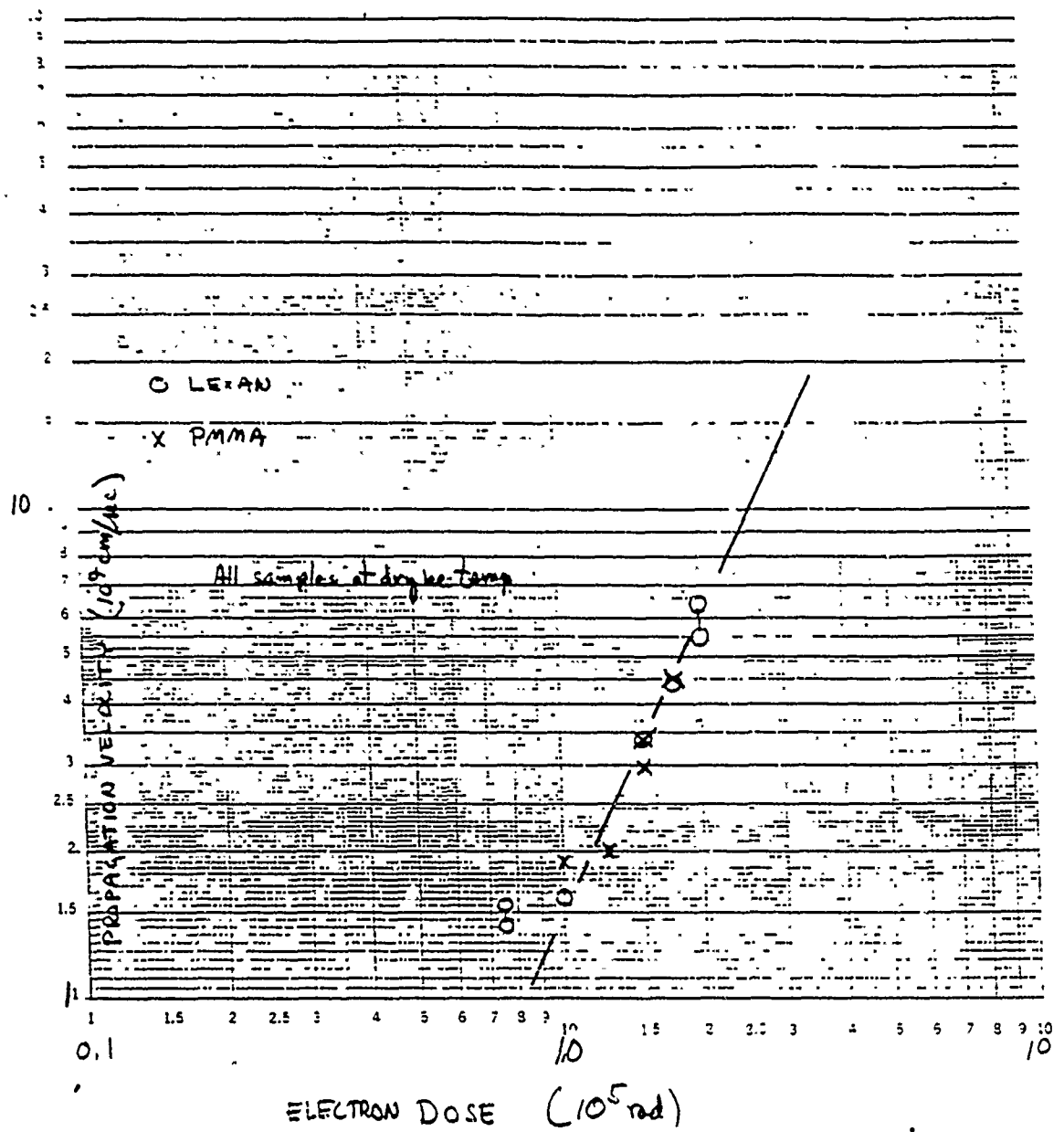


Figure 17 Channel Development Propagation Velocity

MIT-HURL

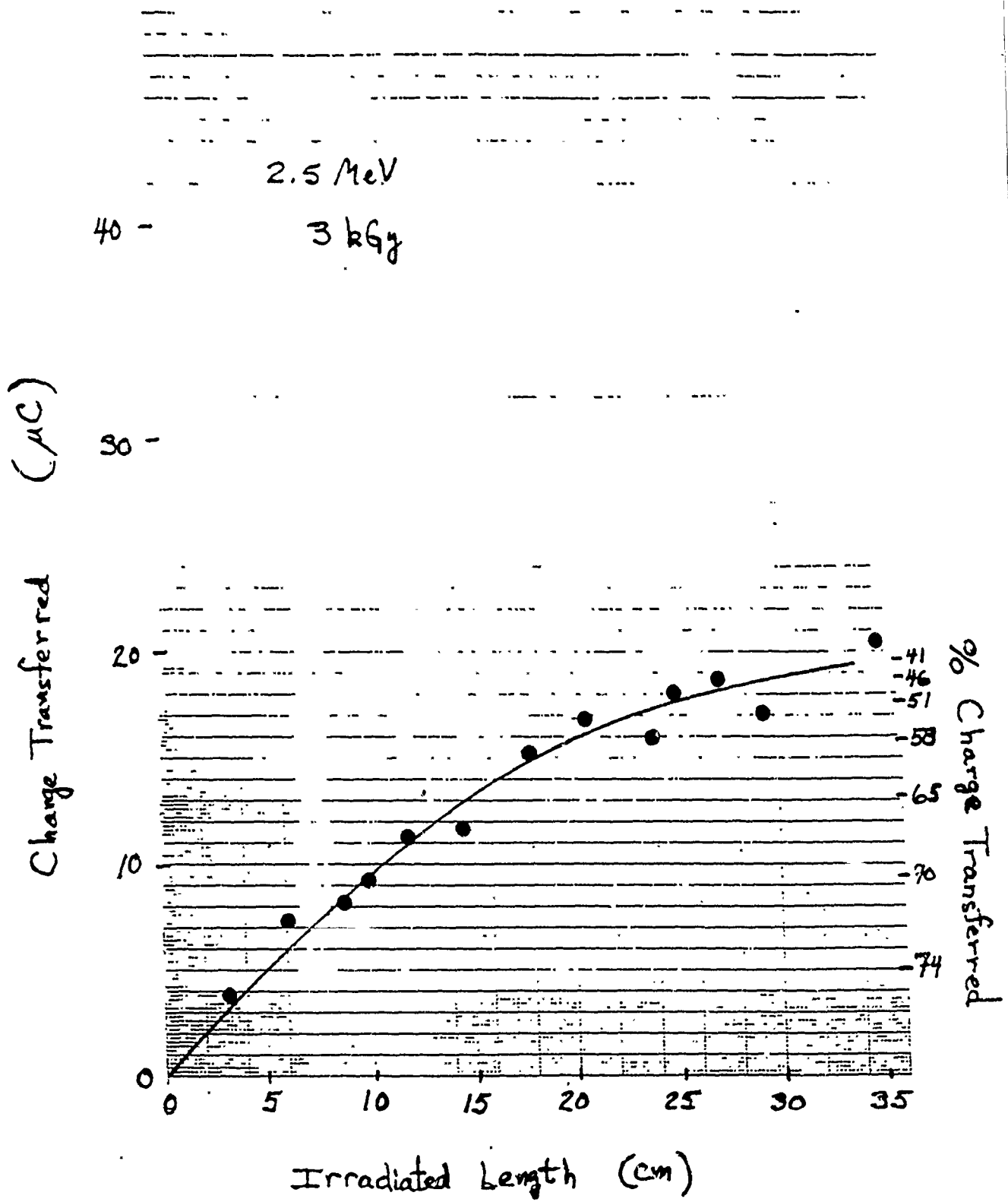


Figure 18 Transferred Charge in PMMA

MIT-HURL

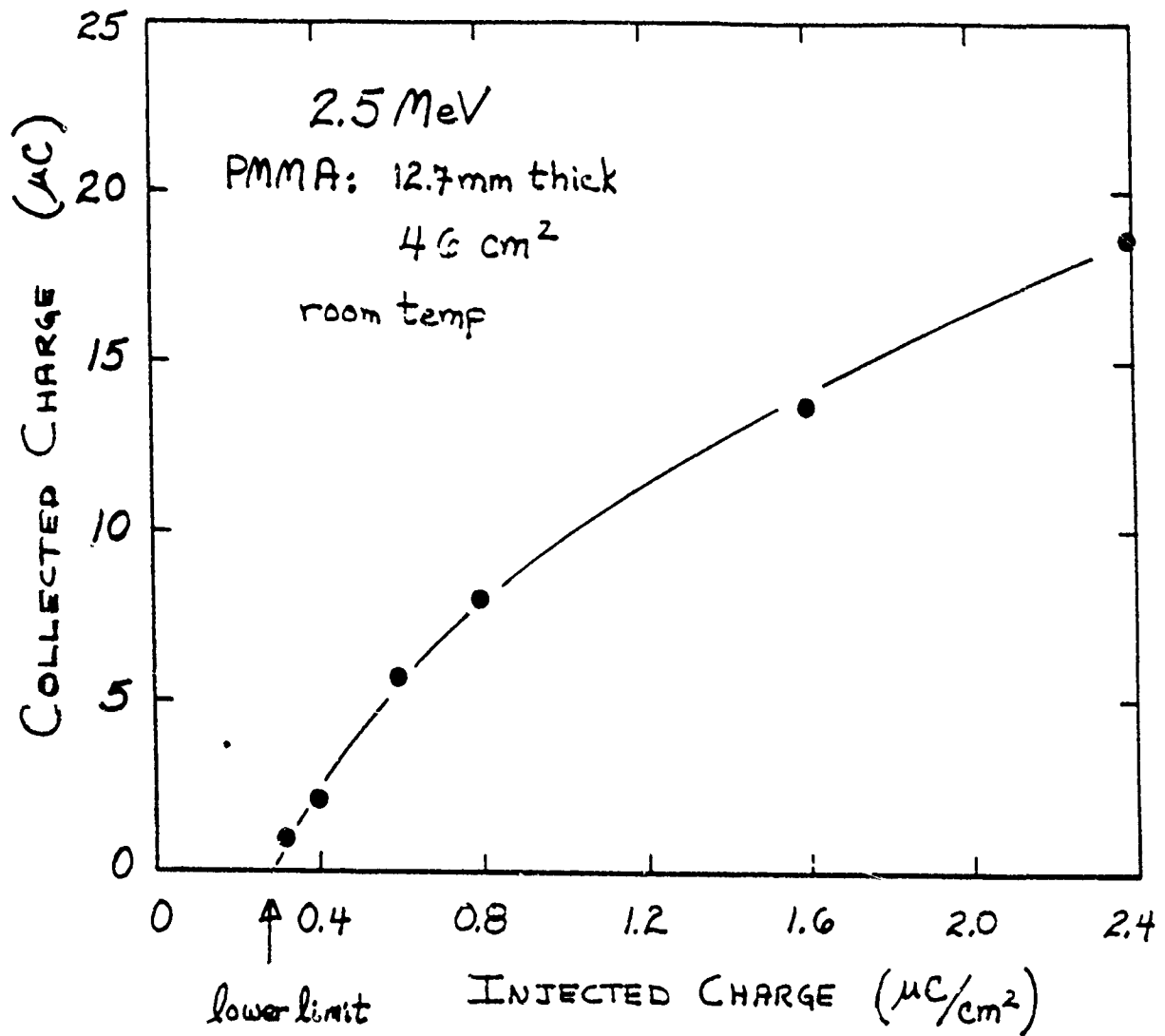


Figure 19 Charge Collection Efficiency for 46 cm² round Charged Area, PMMA

3.2.6 Incident flux rate effects

By modification of the intensity of the e-beam it was possible to change the rate at which charge was implanted in the experimental samples. The electro-acoustic method was used to examine the effect on the internal charge accumulation. Figure 20 shows the measured internal charge vs the total incident e-beam charge. Four different intensities were used (as indicated by the numbers beside the data points). At low incident charge levels, much of the charge is trapped and there is a linear increase of stored charge with trapped internal charge. However, at higher incident charges less of the charge is accumulated.

The lower efficiency of charge trapping at the higher implant intensities can be expected from the characteristics of charge transport. At the higher intensities a greater amount of power is delivered to the sample and heating occurs. But there is a strong dependence of charge transport on temperature, as shown in Section 4.1.2, so that during the charge implant time a significant amount of charge is conducted from the volume by transport. A second means by which reduced net charge is accumulated at high implant rates is due to radiation induced conductivity. The usual model for this effect is that this form of conductivity is proportional to radiation dose rate. Hence, at high implant rates a greater percentage of the injected charge is conducted from the volume.

3.3 Material Effects

In this section the influence of the dielectric material on the channel development is discussed.

3.3.1 Initiation, channel propagation

There is a substantial difference in the amount and morphology of the branched discharge channels which develop in space charged regions according to the dielectric material. These differences will be discussed, but first it is worth pointing out that the basic structure of this class of discharges is remarkably the same, independent of material. Specifically all materials studied show common fundamental characteristics of:

- the sudden formation of channel discharges at sufficient charge levels
- greater ability to accumulate charge at lower temperatures
- light emitted during channel development
- similar velocities of propagation
- discharge channels which do not recross a region during one event
- triggering of discharge by local high electric fields
- e-beam caused space charge accumulation
- increased depth of channels below surface with greater implant energy

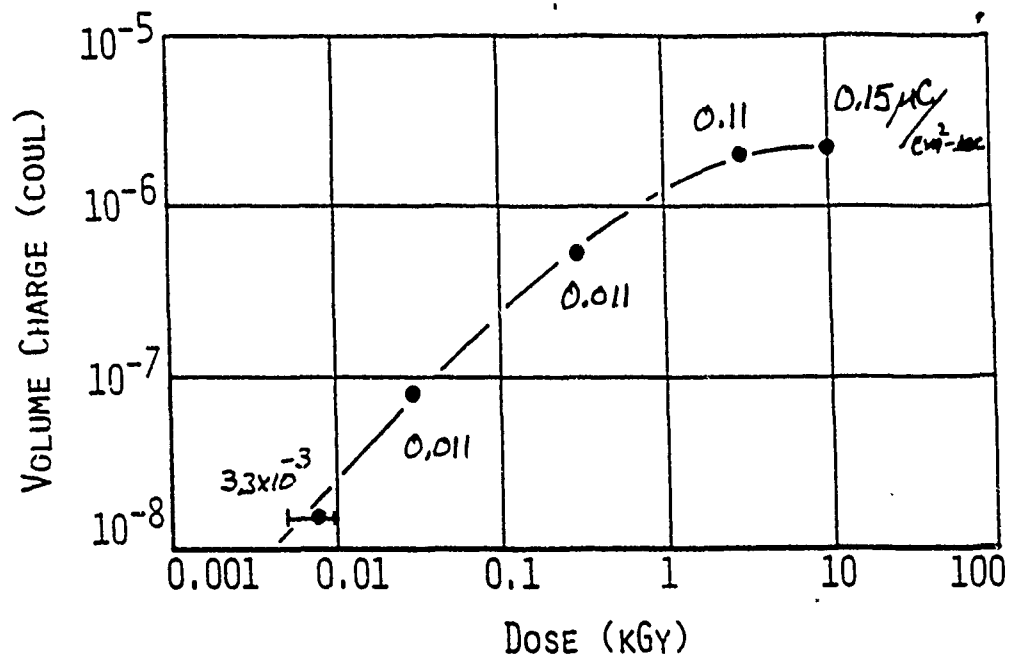


FIGURE 20 INITIAL TRAPPED CHARGE FROM 1 MEV ELECTRONS IN PMMA

MIT-HVRL

The differences associated with materials are most notable in three categories:

- initiation condition
- propagation extent
- channel damage morphology

The cause for these differences seems to be associated with two processes: the charge accumulation physics and the channel plasma physics and damage. The charge accumulation at room temperature in materials such as epoxy can be very small compared to PMMA. However, with epoxy it was possible to obtain sufficient stored charges to cause channel discharges by first cooling the sample to -78°C . The difference in charge storage accounts for the initiation and some of the propagation differences among the different materials.

The propagation extent is determined not only by the amount of space charge available, but also apparently by the conductivity of the channel during propagation. For example, polycarbonate (LEXAN) forms black (carbon looking) channels and this material exhibits unusually long channels, even for charge levels slightly above threshold values. This is interpreted to mean that the channel impedance is low even for long channels and hence discharge propagation can continue because the available energy remains high. Some channels propagated the full length of a 76 cm long sample with only $0.4 \mu\text{C}/\text{cm}^2$ implanted charge. For comparison, the same implanted charge in PMMA yields a channel propagation of just 3.6 cm when it self-stopped.

Surprisingly, even though the propagation length is very different, the velocity of propagation in polycarbonate is similar to that in PMMA. Tests with periodically spaced positions of high charge density, as in Section 3.2.3, showed that the velocities and currents in these materials were different, Figure 21, with the larger values in LEXAN. The higher currents confirm the earlier statement of lower channel impedance in this material. The relative velocity measurements with the 'interferometer' structure, Section 3.2.4, showed a very similar dependence of velocity on implanted charge level, Figure 16.

Not all insulators readily accumulate charges. Polyethylene, for example, is a relatively good dielectric. Yet at room temperature it did not form discharge channels for e-beam intensity values similar to those used in the PMMA or polycarbonate tests. Electro-acoustic measurements showed that the stored charge in polyethylene was indeed orders of magnitude below that of the other two materials. Also the charge decay rate was much higher. Tests were also made with Mylar polyester. However, it was only available in thin sheets so that even at 200 keV beam energy, most of the electrons penetrated the sample. Hence, there was limited charge accumulation and internal discharges did not occur.

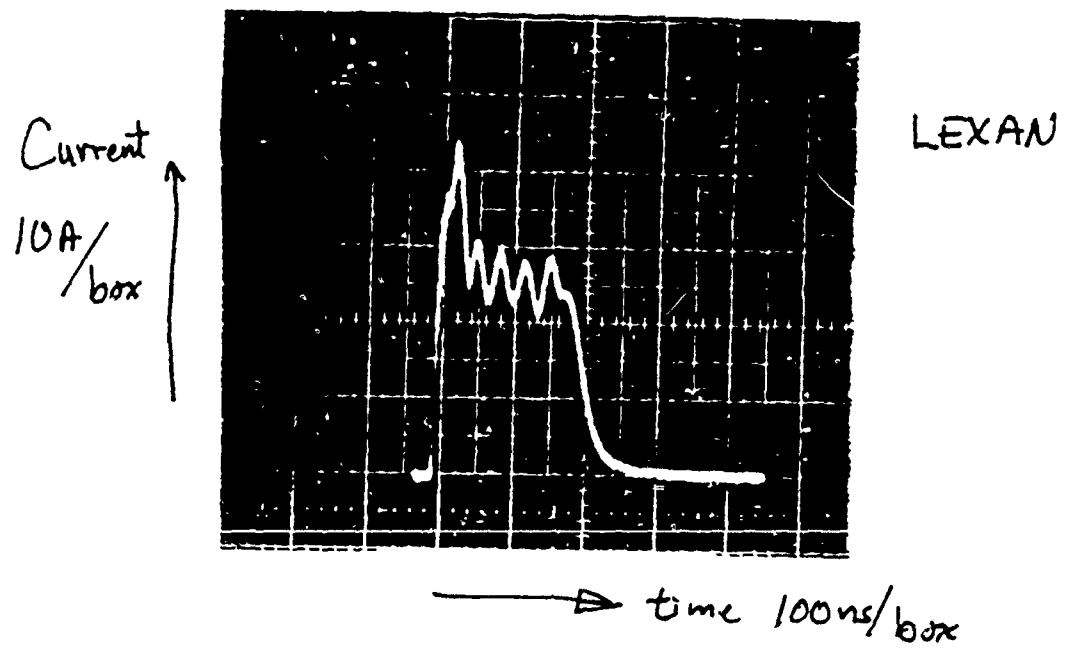
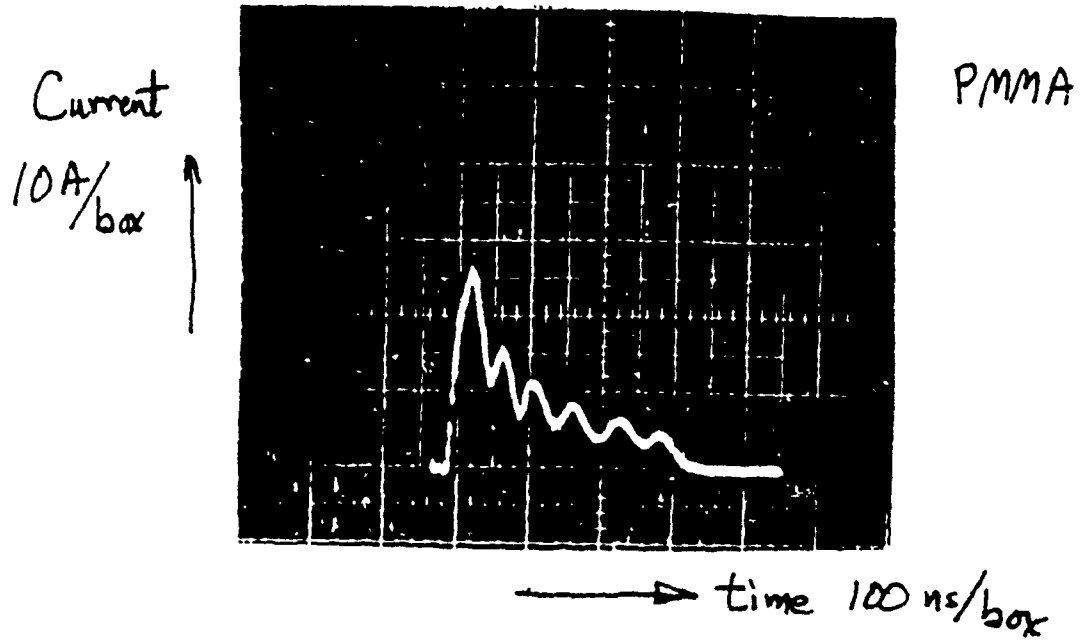


Figure 21 Channel Propagation vs Material₂₆ gap
oscillating charge of $0.6 \mu\text{C}/\text{cm}$, 2.5 MeV

MIT-HURL

3.4 Embedments

3.4.1 Spheres

A sample was made with small 3.2 mm diameter metal spheres embedded in a plane at about the expected depth of the subsequently implanted charge, ie. about 8 to 9 mm below the injection surface. Figure 22 shows the channel structure and the termination of each channel which strikes a sphere. This channeling termination is taken as evidence for a greatly reduced electric tip field due to the larger radius of curvature of the sphere compared to the natural channel tips.

4. MODEL FOR CHARGING OF DIELECTRICS BY E-BEAM IRRADIATION

In this Section the details of a model for the charge accumulation process in solid dielectrics resulting from controlled charge implantation by e-beam irradiation are presented along with experimental results which support the models developed.

4.1 Internal Charge Decay

Assuming that a net charge accumulation within a solid dielectric, such as caused by e-beam irradiation, has occurred, the charge will subsequently move and transport out from the volume. In this section the net charge decay within the dielectric is modelled. This analysis is made in order to understand the net charge which develops during the charging process as well as to understand the subsequent time dependence of changes in volume charges.

4.1.1 Decay with time, initial charge effects

For various initial charge levels within the dielectric, as determined by the e-beam implantation, the decay of net volume charge in samples held at room temperature was measured over a period extending to two months, Figure 23. The samples remained shorted on all sides by wrapping with metal foil during the storage interval between measurements. Two characteristics are readily seen in these curves. First, the relaxation time greatly depends upon incident beam charge. For example, whereas the sample irradiated to (3 kGy) decayed its charge by a factor of 50 in 1,000 hours, the sample irradiated with about (70 Gy) showed less than a factor of 2 charge decay in the same 1,000 hours. Second, all curves appear to extrapolate to a single asymptote of the form $1/8t$, where 8 is a constant $1.6 \times 10^4 \text{ (C-hr)}^{-1}$ and t is time in hours for the 7 cm^2 area.

4.1.2 Temperature effects on decay

Additional samples stored at 60°C and at 90°C were measured for charge relaxation with the same implanted charge of (3 kGy), as that for the reference room temperature test ($\sim 28^\circ\text{C}$). In addition, a sample at dry ice temperature, -80°C , was irradiated to (1.5kGy). The resultant decay curves are shown in Figure 24. Solid lines are drawn with a shift of a factor of 10 for each

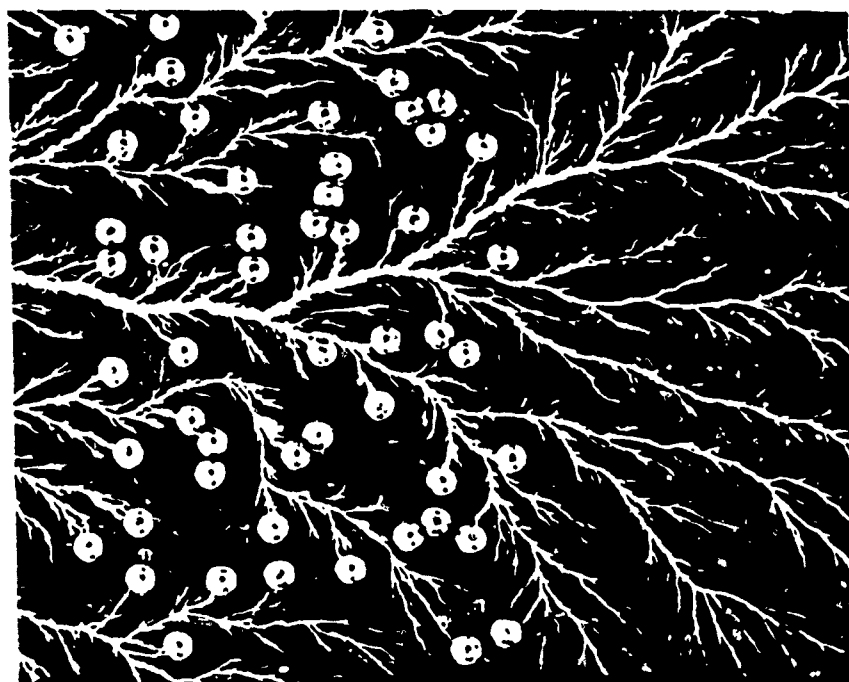


Figure 22 Discharge Channels in PMMA Sample with 3.2mm Dia. Metal Sphere Embedments, Showing Channels Terminate at Spheres

MIT-HURL

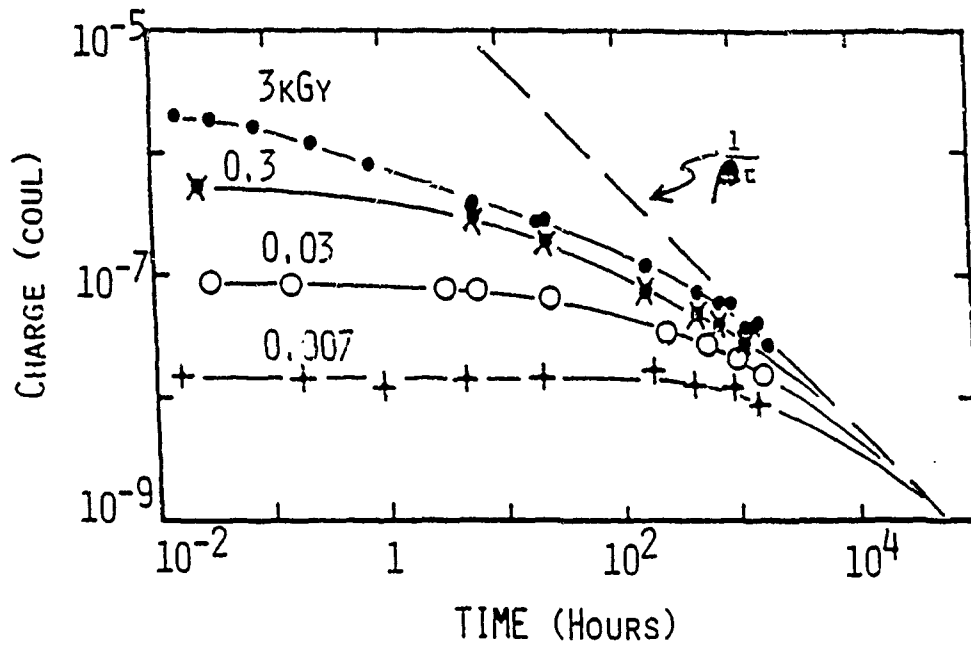


Figure 23 Charge Relaxation in PMMA after Irradiation at 1 MeV

PULSED ELECTRO-ACOUSTIC METHOD FOR THE MEASUREMENT
OF VOLUME CHARGES IN E-BEAM IRRADIATED PMMA

T. Maeno, H. Kushibe, and T. Takada

Musashi Institute of Technology
Tokyo, Japan

and

C. M. Cooke

Massachusetts Institute of Technology
Department of Electrical Engineering
and Computer Science

High Voltage Research Laboratory
Laboratory for Electromagnetic and Electronic Systems
Cambridge, MA 02139

INTRODUCTION

The measurement of volume charges within insulators has been attempted by various methods, including thermal, optical, mechanical, and electrical stimulation of the sample. A new method incorporating pulse electrical stimulation and pulsed acoustic detection is reported here. This technique is an extension of a previously reported [1] high frequency AC steady state electro-acoustic measurements in which electric fields at an electrode surface are determined by measuring the AC high frequency vibration of the electrode in response to a DC plus high frequency AC excitation. The use of pulse operation allows the measurements of time domain delay information which yields the spatial distribution of the volume charge.

In this paper the electro-acoustic pulse method is used to non-destructively probe residual charges remaining in the volume of polymethylmethacrylate (PMMA) samples which have been irradiated with an electron beam. Information about volume charging produced by e-beam irradiation is useful for modelling satellite charging, dosimetry of e-beams such as for medical therapy, and modelling electrical discharges.

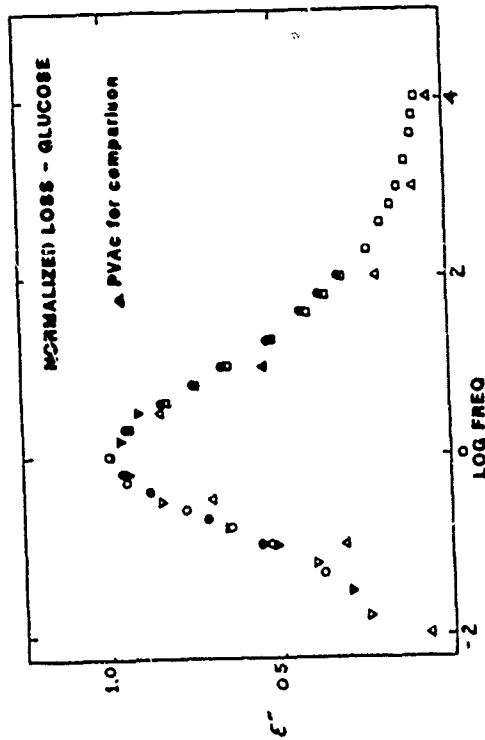


FIGURE 5. NORMALIZED DIELECTRIC LOSS VERSUS FREQUENCY FOR D-GLUCOSE

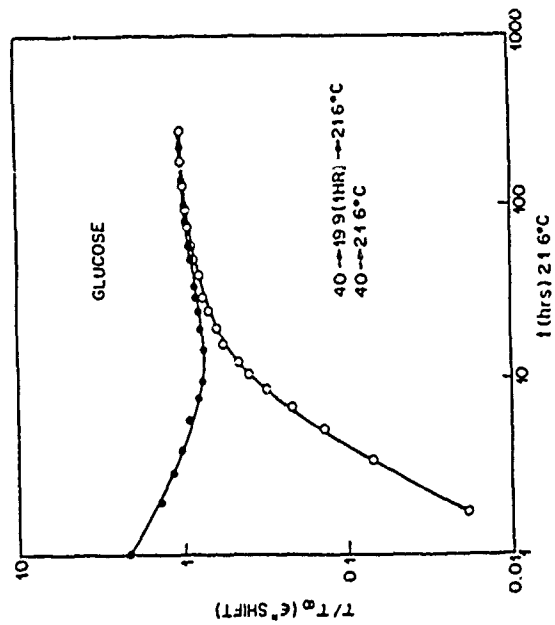


FIGURE 6. "MEMORY EFFECT" IN D-GLUCOSE

ELECTRO-ACOUSTIC STRESS PULSE TECHNIQUE

Consider a charge density, $\rho(x)$ c/m^3 , distributed in a sheet of plastic; then the electric field intensities E_1 and E_2 at each metalized surface of the short circuited sample are given by the following equations: [1]

$$E_1 = -\frac{1}{\epsilon} \int_0^d \frac{d-x}{d} \rho(x) dx \quad (1)$$

$$E_2 = \frac{1}{\epsilon} \int_0^d \frac{x}{d} \rho(x) dx \quad (2)$$

The total charge, Q , and its mean depth, \bar{x} , can be determined from the electrode field values by:

$$Q = S_0 e(E_2 - E_1) \quad (3)$$

$$\bar{x} = \frac{E_2}{E_2 - E_1} d \quad (4)$$

where ϵ is a dielectric constant, S_0 is the electrode area, and d is the thickness of the sheet material.

To determine the intensity and direction of E_1 or E_2 , two steps are needed: first, a pulse E-field is generated uniformly in the sample, and next, the resulting vibrations are detected. A high electric field pulse, e_p , is produced by a high voltage rectangular pulse, v_p , applied across the electrode.

$$e_p = \frac{v_p}{d} [u(t) - u(t-\tau)] \quad (5)$$

where $u(t)$ is the unit step function and τ the pulse width. The electric force density acting on the metalized surface of plate is given as follows:

$$F = \frac{1}{2} e(E+e_p)^2 = \frac{1}{2} eE^2 + eEe_p + \frac{1}{2} ee_p^2 \quad (6)$$

The first term of equation (6) represents the electrostatic force; the second and third terms correspond to the pulsive force.

A piezo-device attached to the rear side of one electrode is employed to detect the acoustic pressure pulse wave at the electrode surface contacting the sample, Figure 1. When $E \gg e_p$, the amount of signal excited from the piezo-device is proportional to the second term of equation (6). The output signal, V_s , is therefore represented by:

$$V_s = K e E \frac{p}{d} \quad (7)$$

where K is a constant which depends upon the transducer and on acoustic coupling. The electric field intensities E_1 and E_2 at each electrode surface can respectively be known from equation (7).

The high voltage pulse generator is adjusted to a $\tau=90$ nsec pulse width so as to excite a resonance frequency of the piezo-device, $f_0=1/\tau$. It is coupled to the electrodes through the 500pF capacitor.

To determine the constant K in equation (7), the relationship between a known electric field E and the signal voltage V_s was obtained. The E was deduced from the ratio a DC voltage applied to a space charge-free sheet material of thickness d . From the results in Figure 2, K is -1.58×10^{-6} V/C, and the relation between V_s and E is:

$$E = -2.1 \times 10^{10} V_s \quad (8)$$

SHEET-CHARGE WITHIN A PMMA PLATE

When an interior sheet-charge, Q_s , lies parallel to the surfaces of a PMMA sample which is held between two grounded electrodes, it induces surface charges of opposite polarity on both electrodes. It also generates an internal electric field intensity at both electrodes, E_1 and E_2 . We used the electro-acoustic pulse technique to investigate a sample which contained a sheet charge. Quantities of interest included interfacial electric field intensity at each electrode, E_1 and E_2 , the amount and polarity of sheet-charge Q_s , and its position, \bar{x} .

An assembly of two PMMA sheet samples of 2 and 3mm thickness was inserted between electrodes, as shown in Figure 3. Both sides of each sheet had a vacuum evaporated aluminum electrode. After depositing the electrodes, the two sheets were attached together with dichloromethane so as to yield a center electrode and two outer electrodes. The adhesive helped prevent reflections of acoustic pulses due to the interface. A charging voltage of $V_0 = -14\text{KV}$ on the center electrode relative to the grounded outer electrodes induced a negative sheet charge, $Q_s = -0.25 \times 10^{-6}\text{C}$, as shown in Figure 3.

A high voltage pulse, $V_p = 5\text{KV}$ and width $\tau = 90\text{nsec}$, was applied to the electrodes to excite acoustic pulses from the charges at the outer electrodes and the sheet-charge layer. The piezo-device produces electric signals V_{s1} , V_{s2} , V_{s3} , from the acoustic pulses at respective delay times t_1 , t_2 , t_3 , in the order as shown in Figure 3 and the scope trace in Figure 4.

The acoustic velocities in an aluminum electrode and the PMMA sheet sample, V_{A1} and V_{PMMA} , listed in Table 1 can be estimated from a relation between the travelling distance l and time t_1 . These velocities are nearly equal to published values. [2] The transit time-interval ratio of $(t_2 - t_1)$ to $(t_3 - t_1)$ between the three pulses V_{s1} , V_{s2} , V_{s3} , is, furthermore, very close to the ratio of specimen thickness d_1 to d_2 . The electrical signals V_{s1} , V_{s2} , V_{s3} , according to the above two results, coincide with the pulsive acoustic pressures and polarity coming from the positive induced charge at $x=0$, the negative sheet charge at $x=d_1$, and the positive one at $x=d_1+d_2$, respectively. The electric field intensities, E_1 and E_2 , can be obtained from substitution V_{s1} and V_{s3} into equation (8). These are all in good agreement with the electric field intensities calculated from the relation between the charging voltage V_0 and thickness of specimen d_1 or d_2 .

ELECTRON BEAM IRRADIATED PMMA

A monoenergetic electron beam from a Van de Graaff generator was used to irradiate PMMA samples. The interior trapped charge remaining after irradiation was

determined using the electro-acoustic pulse technique. The PMMA specimens were square, 50mm on a side, and 5mm thick with deposited aluminum electrodes, 30mm in diameter in the center of the two faces.

Typical waveforms obtained before and after irradiation are shown in Figure 5. In each of these, V_{s1} is the pulse from the electrode on the irradiated side, V_{s2} is the pulse from the charge layer, and V_{s3} is the pulse from the electrode on the opposite side of the sample. The non-irradiated sample shows no initial charge in the sample, Figure 5a. Irradiation at 1MeV beam energy shows a negative charge layer at a depth of about 2.6mm, Figure 5b. At 1.5MeV beam energy, the charge penetrates deeper and the negative layer is seen to be building up as the beam exits the opposite side of the sample, Figure 5c. And at 2.0MeV, Figure 5d, the beam easily penetrates the sample, but of course some residual negative charges remain as directly seen by the positive image charges on the electrodes. The average depth of these charges appears to be about 3mm. The penetration of the 5mm thick PMMA sample by a beam of 1.5MeV energy corresponds well to the published values of 1.2 to 1.4MeV for a 5mm range in plastic. [3,4]

A series of tests made with three energies and three dose levels showed a reduction in accumulated charge at high doses of 10 Mrads, Figure 6. In contrast, at low doses, the volume charge is known to increase with dose. [4] However, for the multimegarad case, enhanced conductivity caused by the irradiation and by heating of the sample will lower the resultant volume charge. More needs to be known about the charging during the irradiation period and the speed of decay immediately after the beam is stopped to distinguish total dose and dose rate effects.

CONCLUSION

The non-destructive electro-acoustic pulse technique has been developed and applied to confirm the amount and distribution of accumulated charge in PMMA resulting from e-beam irradiation. For beam energies with ranges well below the sample thickness, a concentrated negative charge layer is seen. And for beam energies with ranges well above the sample thickness, a broadly distributed negative charge remains.

REFERENCES

1. Takada, T., and T. Sakai, "Measurement of Electric Fields at a Dielectrode/Electrode Interface Using an Acoustic Transducer Technique," *IEEE Trans. EI-18*, 619 (1983).
2. Saneyoshi, J., K. Kikuchi, and O. Nohmoto, *Handbook of Ultrasonic Wave Techniques*, 1325, 1353 (1973) (Japanese).
3. Kobetich, E. J., and R. Katz, "Energy Deposition by Electron Beams and γ rays," *Phys. Rev.* **170**, 391 (1968).
4. Cooke, C. M., E. Williams, and K. A. Wright, "Electrical Discharge Propagation in Space Charged PMMA," *IEEE International Symp. on Elect. Insul.*, Philadelphia, PA, 95 (1982).

ACKNOWLEDGMENT

The contributions of C. M. Cooke have benefited from the support of the Air Force Office of Scientific Research.

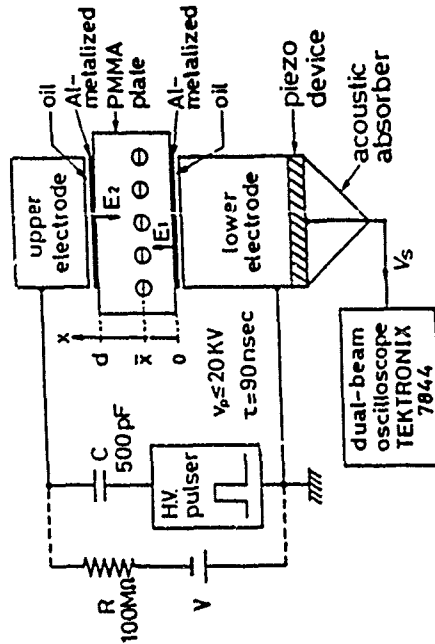


Figure 1. Electro-acoustic Pulse Measurement System

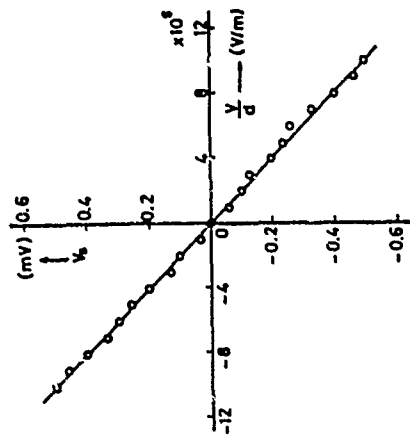


Figure 2. Calibration Acoustic Pulse Signal Versus Electric Field Value

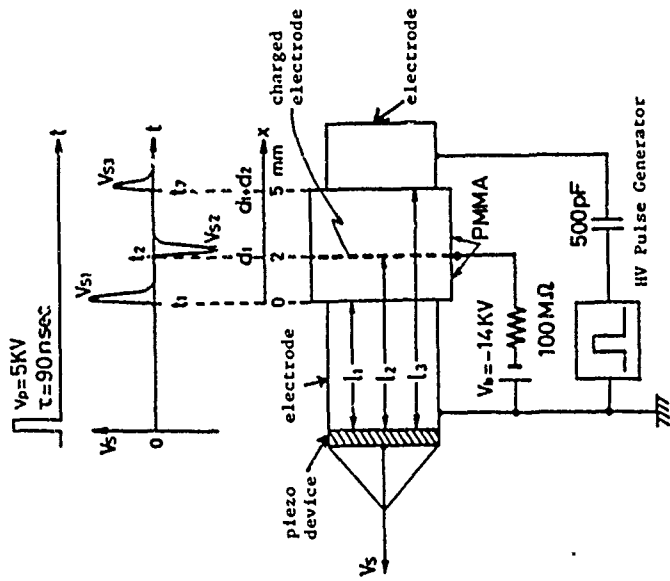


Figure 3. Travelling Wave Acoustic Pulses with Charge Layer

TABLE I

Calibration of Detector with Charged Sheet in PMMA

Sample thickness	Given data	Measured data
d_1 d_2	2.0 mm 3.0 mm	$\bar{x} = 1.93$ mm 3.07 mm
Acoustic path length	l_1 l_2 l_3	— — —
Charging voltage	V_b	—
Accumulated charge	Q	-0.26×10^{-8} C
Electric field	$E_1 = -V_b/d_1$ $E_2 = -V_b/d_2$	7.0×10^6 V/m -4.82×10^6 V/m
Delayed time	t_1 t_2 t_3	3.82 msec 4.62 msec 5.82 msec
Signal height	V_{S1} V_{S2} V_{S3}	350 μ V -4.0 μ V 220 μ V
Acoustic velocity	$V_{A1} = l_1/t_1$ $V_{A2} = l_2/t_2$ $V_{A3} = l_3/t_3$	6260 m/sec 2720 m/sec

* given in reference [2]

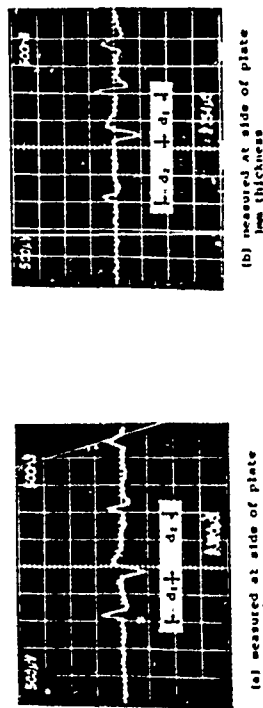


Figure 4. Acoustic Signal Waveforms for Charge Layer in PMMA

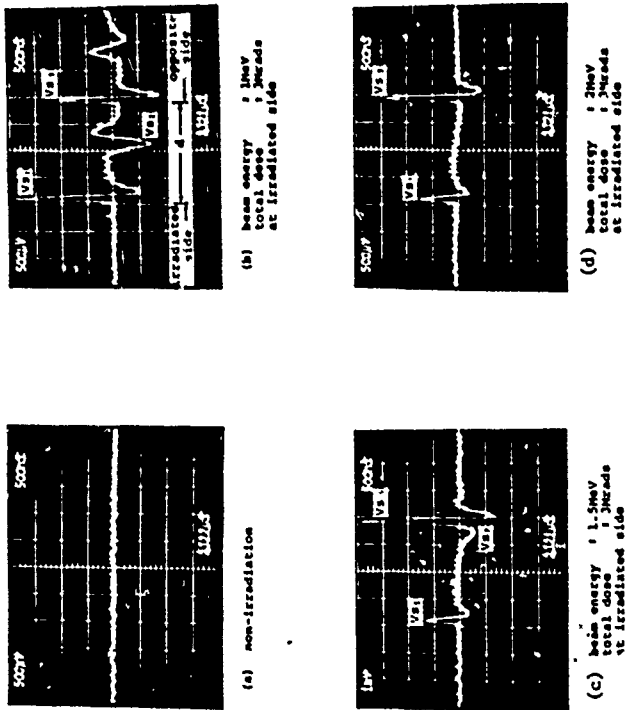


Figure 5. Acoustic Signal Waveforms for E-beam Charged PMMA

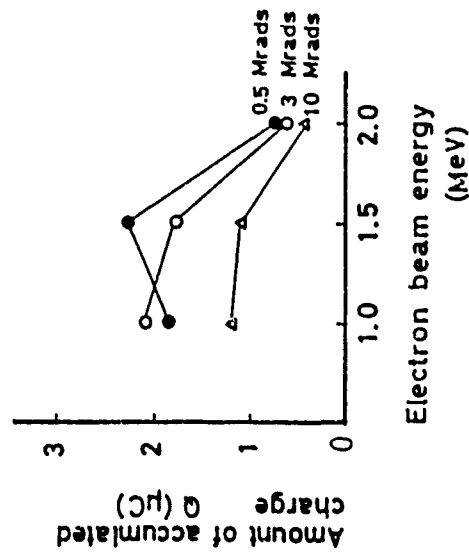


Figure 6. Accumulated Charge Versus E-Beam Dose in PMMA

SPACE CHARGE ACCUMULATION IN POLYMETHYLMETHACRYLATE
RESULTING FROM ELECTRON BEAM IRRADIATION

C.M. Cooke, M. Zahn, K.A. Wright, and M. Hikita
Massachusetts Institute of Technology
Laboratory for Electromagnetic and Electronic Systems
High Voltage Research Laboratory
Cambridge, MA 02139

INTRODUCTION

The measurement of volume charges within insulators provides needed information important to spacecraft application. The actual charge values help in establishing models for charge accumulation and decay and lead to a better understanding of spontaneous discharges of insulators exposed to energetic electron irradiation. In this work, two methods of measurement of trapped charges in polymethylmethacrylate are used; the electro-acoustic method [1] and the Kerr electro-optic method [2]. Both provide quantitative information about internal space charges.

Of particular interest are the volume charges in PMMA resulting from exposure to megavolt energy electrons [3,4,5,6]. A series of tests were made to determine how charges accumulate according to dose, what are typical profiles of charge with depth into the bulk material, and what are typical relaxation decay times for this charge to leave the sample.

EXPERIMENTAL METHOD

The electro-acoustic method yields volume charge information by applying a short pulse electric field to the sample and measuring the resultant mechanical pressure wave which arrives at the electrodes [1,7]. The shock magnitude and time delay of arrival are measured with a piezoelectric transducer and provide information about the size and distribution of the volume charge. Figure 1 shows a schematic of this type of system.

The Kerr method employs incident light polarized at 45° to the direction of the electric field in the sample and an analyzing polarizer placed after the sample. [2,5] The resultant transmitted light intensity is a function of the internal field and when uniformly illuminated provides a complete field intensity map over the depth of the sample. Figure 2 shows a schematic of apparatus for the Kerr measurements.

Both methods as a practical matter need a calibration constant. This is determined by means of tests with a known applied field [2,7]. With the separately determined constants, the measurements become quantitative.

The measurements were made on PMMA samples typically 0.6 to 1.3cm thick. Electrons from a Van de Graaff generator entered the sample on the broad area face with energies in the 0.5 to 2.5MeV range with current densities 5 to $250\text{nA}/\text{cm}^2$. The samples had thin metal foil electrodes which short-circuited top and bottom faces throughout the tests.

VOLUME CHARGE ACCUMULATION

The net accumulation of charge within the samples when at room temperature was determined by the electro-acoustic method and was found to increase linearly with dose up to about 0.1 or 0.2 kGy. At higher doses, a saturation-type response occurs, Figure 3. This may result from one or more of the following processes: space charge repulsion by the already trapped volume charge, radiation induced conductivity, and/or heating which reduces relaxation times.

VOLUME CHARGE PROFILE

The electro-optical method was used to reveal the distribution of volume charges by virtue of the electric fields which they induce. Figure 4 shows a typical measured field distribution for 2MeV electrons incident on a 12.7mm thick sample. The influence of incident beam energy is shown in Figure 5,

where the depth for zero field, i.e., the point of internal voltage maximum, is plotted against beam energy. A linear increase of depth with energy occurs in this case where the sample is thicker than the electron range. Note the measured distribution is very close to that theoretically predicted by Tanaka, et al. [8] and to measurements obtained with collecting plates [9], which is good confirmation of the results.

VOLUME CHARGE DECAY

The electro-acoustic method was used to measure the remaining net charge as a function of time after a given short-term injection of charge. Figure 6 shows the results for the case of decay after incidence of a 1.0MeV beam to a level of 10^{-6} coul/cm². The decay to half-value occurred in about 25 to 30 minutes, but decay to one-tenth initial value took about 70 hours. Reduction by a factor of 100 is extrapolated to about 3,000 hours. This is a non-exponential decay and at longer times follows the self-precipitation model of a $(t+\tau)^{-1}$ time dependence.

CONCLUSIONS

Volume space charge accumulation in the insulating dielectric PMMA has been shown to occur as a result of electron irradiation. At low doses the net charge increases linearly with dose, but charge decay can be significant and acts to continuously discharge the sample. At high doses, a saturation of net charge occurs quickly. At low and moderate doses, the charge profile in depth appears to be consistent with model predictions.

ACKNOWLEDGEMENT

This work has been supported by the Air Force Weapons Laboratory via the Computer Sciences Corporation and by the Air Force Office of Scientific Research.

REFERENCES

- [1] Maeno, T., H. Kushibe, T. Takada, and C.M. Cooke, "Pulsed Electro-acoustic Method for the Measurement of Volume Charges in E-Beam Irradiated PMMA," 1985 Annual Report Conf. on Electrical Insulation and Dielectric Phenomena, 389-397.
- [2] Kim, K.S., T.C. Cheng, and D.E. Cooper, "Kerr Effect in Solid Polymethylmethacrylate and Polyethylene," J. Appl. Phys. 54(1), 449-451 (1983).
- [3] Trump, J.G., and K.A. Wright, "Injection of Megavolt Electrons into Solid Dielectrics," Mat. Res. Bull. 6, 1075-1084 (1971).
- [4] Cooke, C.M., E. Williams, and K.A. Wright, "Electrical Discharge Propagation in Space-Charged PMMA," Proc. IEEE Internat. Symposium on Electrical Insulation, 95, Philadelphia, PA, June 1982.
- [5] Zahn, M., M. Hikita, K.A. Wright, and C.M. Cooke, "Kerr Electro-optic Field Mapping Measurements in Electron Beam Irradiated Polymethylmethacrylate," to be pres. at Second Internat. Conf. on Conduction and Breakdown in Solid Dielectrics, Erlangen, Germany, July 7-10, 1986.
- [6] Cooke, C.M., T. Maeno, H. Kushibe, and T. Takada, "Pulsed Electro-acoustic Determination of Self-Relaxation of MeV Energy Implanted Electron Charge in PMMA," to be pres. at Second Internat. Conf. on Conduction and Breakdown in Solid Dielectrics, Erlangen, Germany, July 7-10, 1986.
- [7] Takada, T., T. Maeno, and H. Kushibe, "An Electric Stress Pulse Technique for the Measurement of Charges in a Plastic Plate Irradiated by an Electron Beam," Proc. Fifth IEEE Internat. Symp. Electrets, 450-455, Heidelberg, Germany, 1985.
- [8] Tanaka, R., et al., "The Effect of Accumulated Charge on Depth Dose Profile in Polymethylmethacrylate Irradiated with Fast Electron Beam," IEEE Trans. on Nuc. Sci. 26, 4670 (1979).

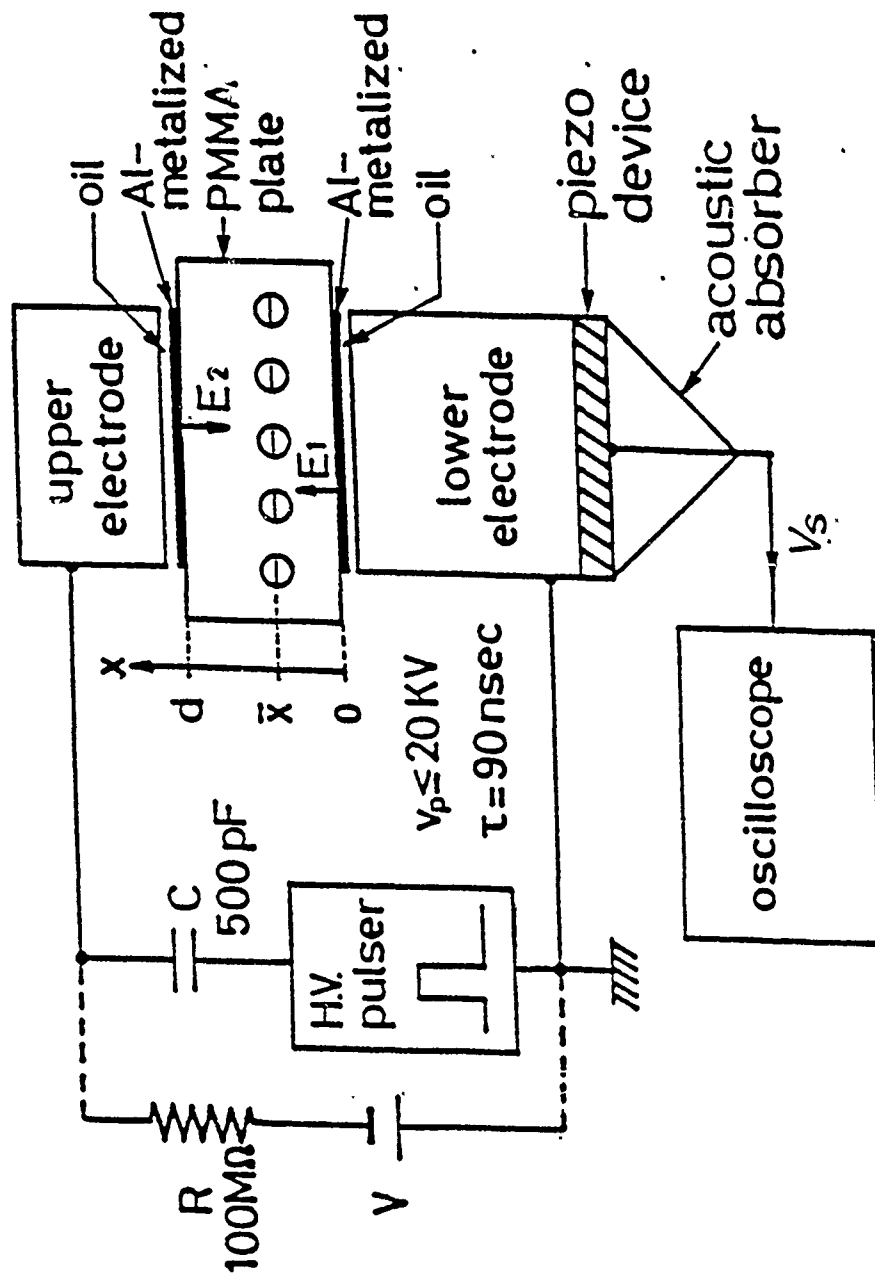


Figure 1. Electro-acoustic Pulse Measurement System

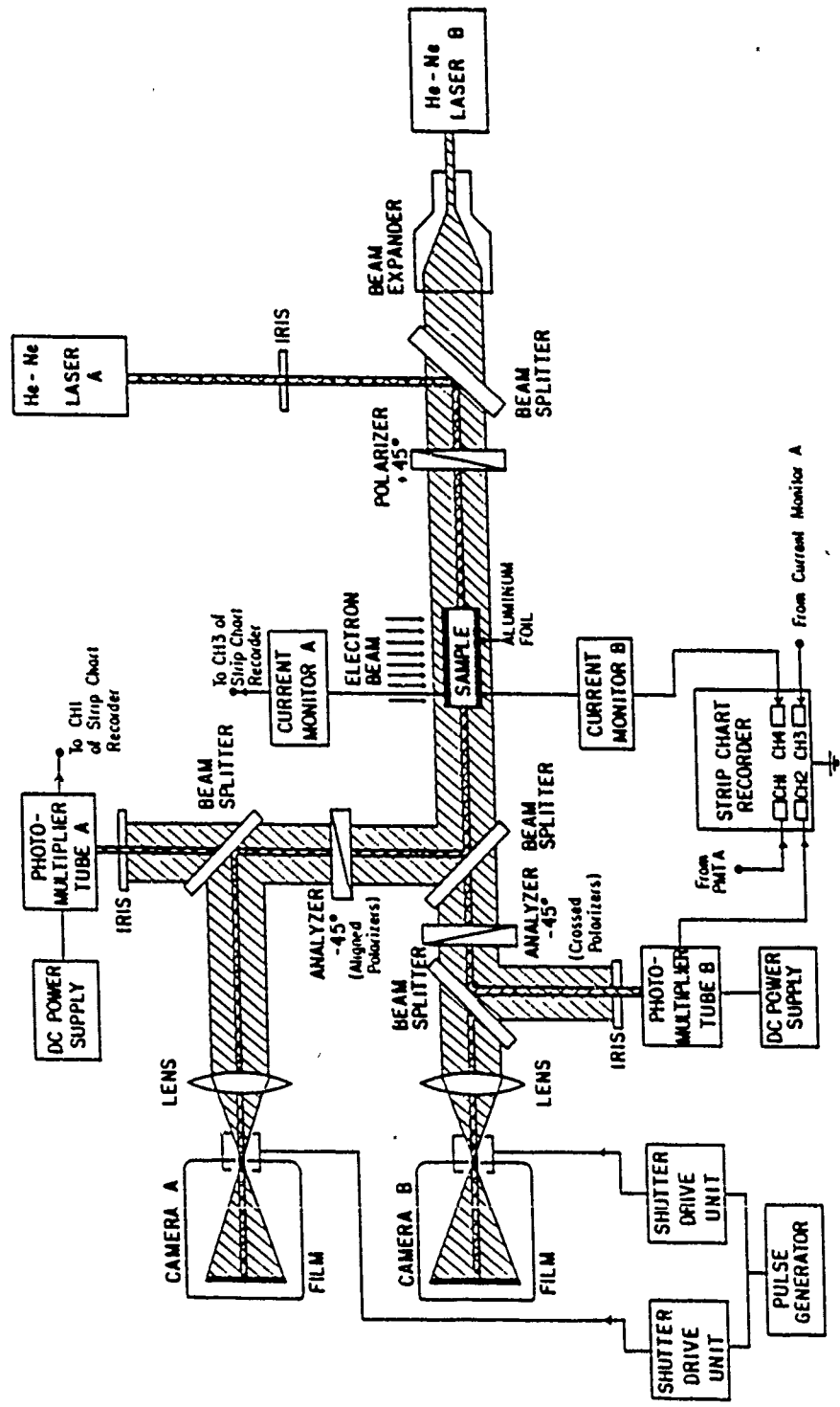


FIGURE 2. ELECTRO-OPTIC MEASUREMENT SYSTEM

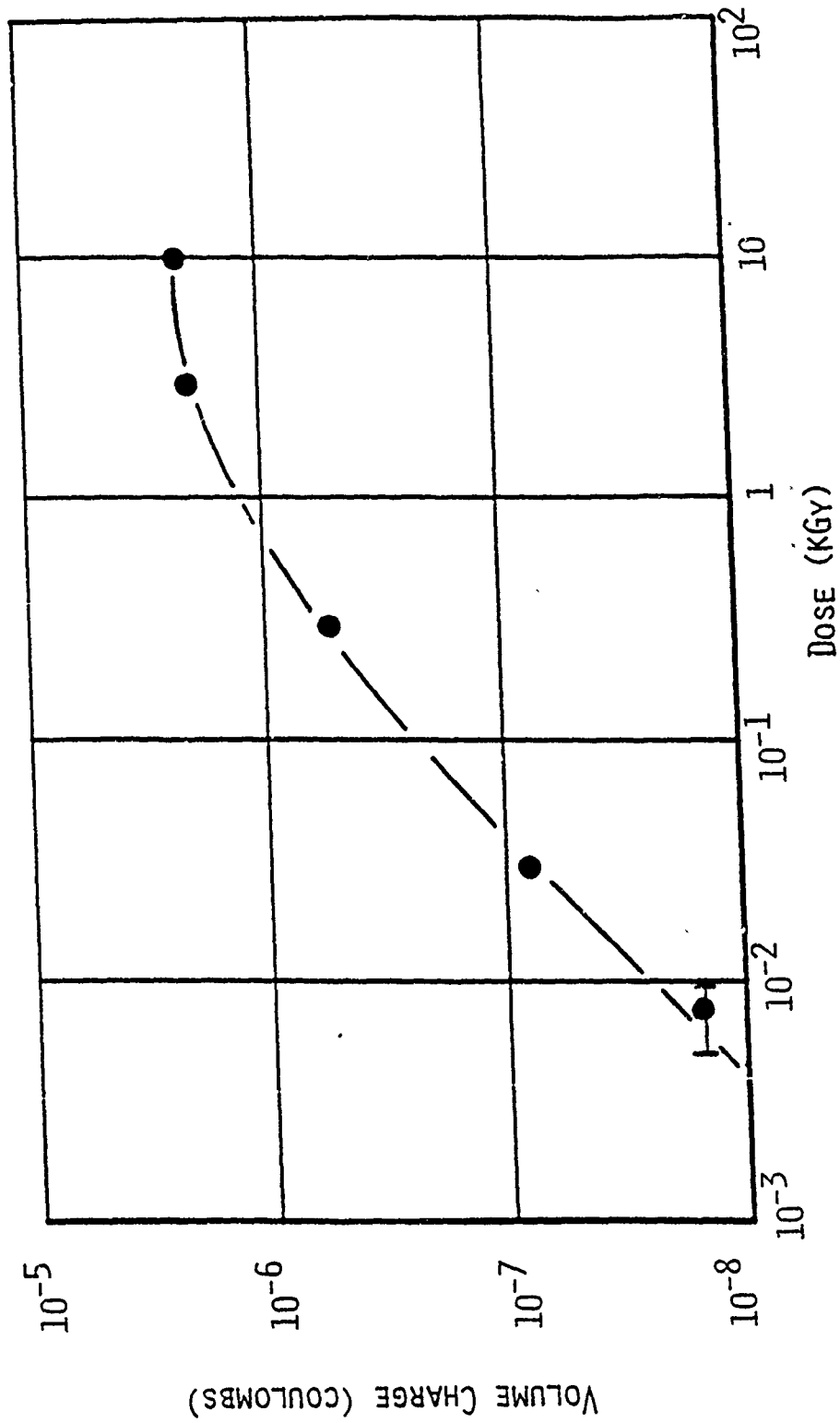


FIGURE 3. MEASURED INITIAL TRAPPED CHARGE FROM 1 MEV ELECTRON IN PMMA,
ELECTRO-ACOUSTIC METHOD GROUPED SURFACES

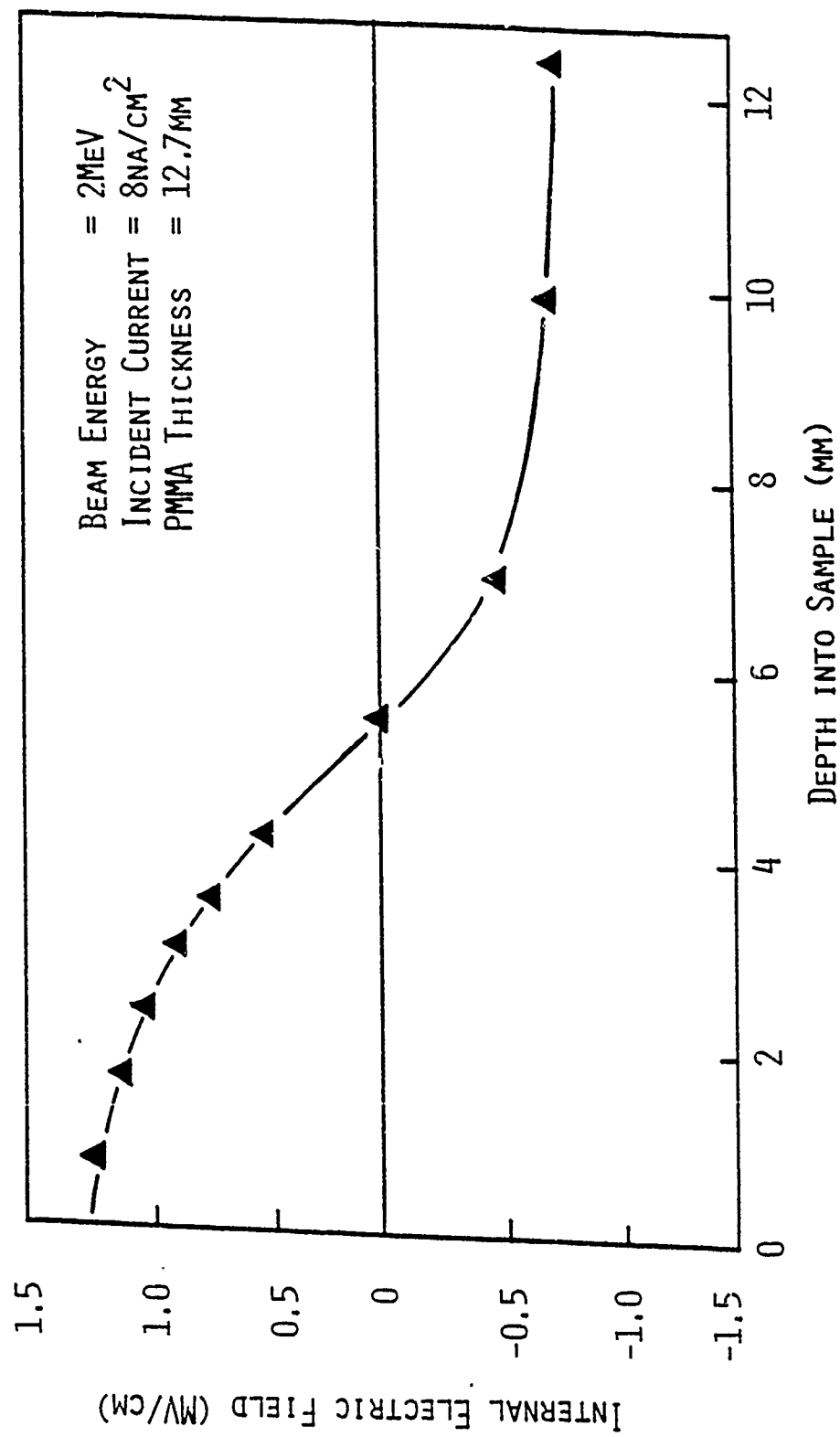


FIGURE 4. DISTRIBUTION OF ELECTRIC FIELD IN PMMA AFTER IRRADIATION
 WITH 2 MEV ELECTRONS MEASURED WITH ELECTRO-OPTIC METHOD.

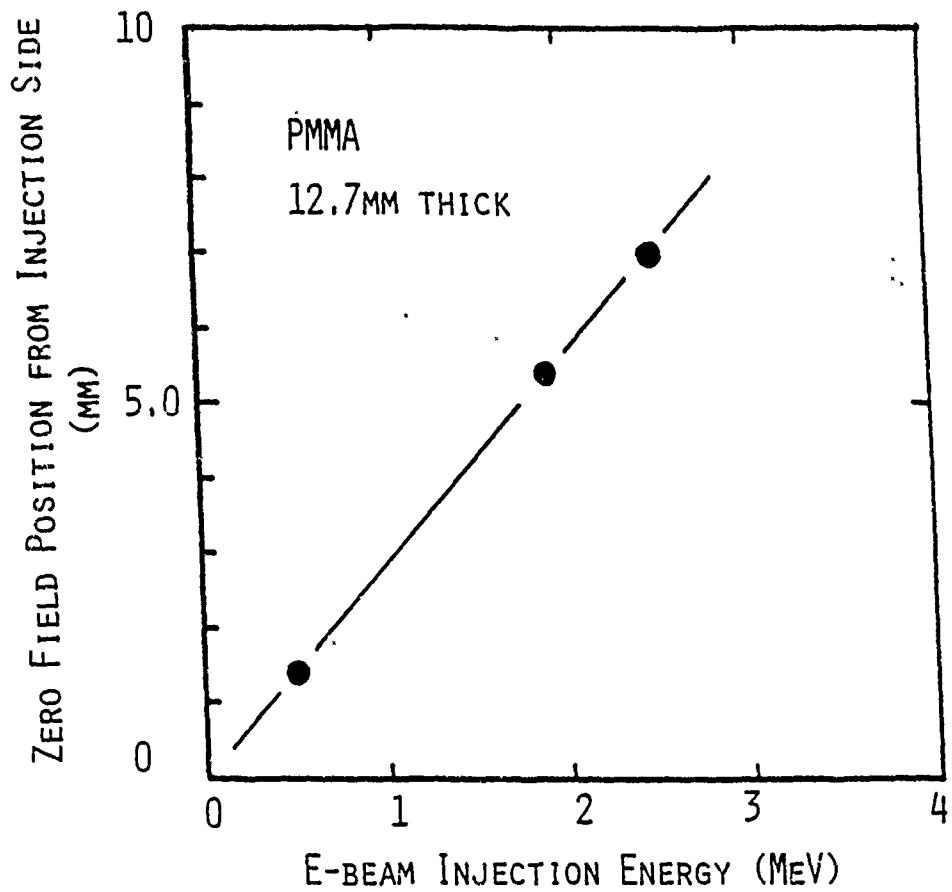


FIGURE 5. DEPTH INTO PMMA FOR ZERO ELECTRIC FIELD, GROUNDED SURFACES, 5 TO 220NA/CM², FIELDS ABOUT 1 MV/CM

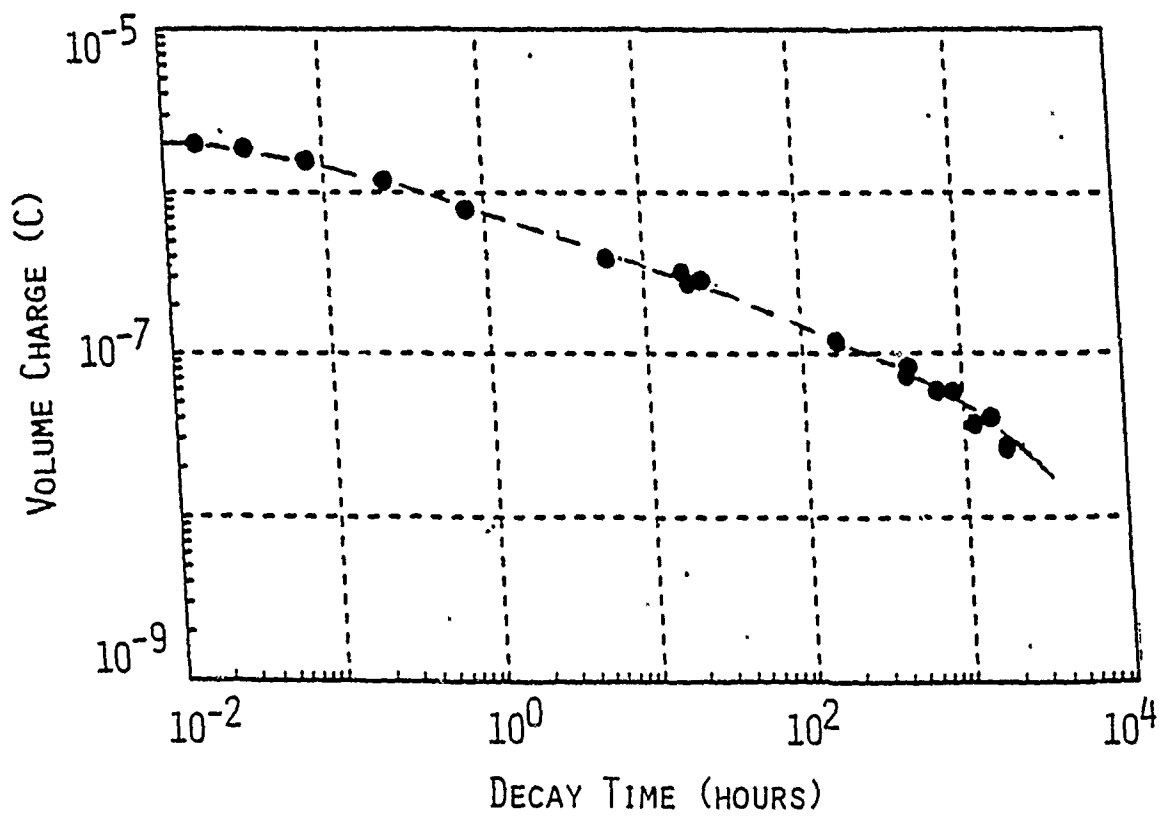


FIGURE 6. VOLUME CHARGE DECAY IN PMMA AFTER IRRADIATION WITH 1 MeV ELECTRONS TO 3 kGY IN 10SEC, ELECTRO-ACOUSTIC METHOD 5 CM² SAMPLE AREA

2nd IEEE Conf. on Conduction and Breakdown
in Solid Dielectrics July 1986

PULSED ELECTRO-ACOUSTIC DETERMINATION OF SELF RELAXATION
OF MeV ENERGY ELECTRONS IMPLANTED CHARGE IN PMMA

C.M. Cooke and K.A. Wright
Massachusetts Institute of Technology
Laboratory for Electromagnetic and Electronic Systems
High Voltage Research Laboratory
Cambridge, MA 02139, U.S.A.

and
T. Maeno, H. Kushibe, and T. Takada
Musashi Institute of Technology
Tokyo, Japan

I. Introduction

Volume charge distributed within insulating media can occur during normal usage of dielectric materials or as an intentional perturbation, introduced to probe the physical conduction processes. For the former case, net charge may accumulate internally from non-uniform conductivity [1], because of injection at electrode-dielectric interfaces, from static electrification effects with flowing oil, or from exposure to energetic radiation. Examples of these occur in HV power cables and supports, capacitors, transformers, spacecraft, nuclear power station apparatus, and medical diagnostic equipment, respectively.

Intentional charge injection is a well-known diagnostic method for the study of conduction in semiconductors. Carriers are released locally, and then their drift and diffusion in the material are detected. In the semiconductor case the charge motion is usually fast enough to allow detection by straightforward current measurements. In relatively good dielectrics, charge transport can be so slow that current measurements are awkward and direct indications of the contained charge is highly preferred.

A series of experiments was performed to study charge motion and self-relaxation in the highly insulating material polymethylmethacrylate (PMMA). This

investigation employed the direct injection of energetic electrons from a Van de Graaff accelerator into PMMA to produce net volume charges. A new method, the pulsed electro-acoustic technique [2], was used to detect and monitor the volume charges. Two major parameters, the initial charge and the sample temperature, were varied to help model and quantify the charge transport dynamics. The samples were monitored for periods as long as months and contained initial charges as high as $1/2 \mu\text{coul/cm}^2$ with resultant fields of about 1 MV/cm.

II. Experimental Method

The samples employed in this work were all square, 50mm on a side, and 7.86mm thick. The central region of each face side was metallized with aluminum in a 30mm dia circle, 7cm^2 area. The electron beam entered through the top side while the electrodes on both top and bottom sides were grounded, Figure 1. The electron irradiation was uniform over the sample in open air, with 40cm of air path from the accelerator exit window to the sample surface. The accelerator was a Van de Graaff machine set with a terminal energy of 1.0 MeV in these studies. Because of energy loss in the air path and thin metal window, the incident beam energy of the sample is closer to 0.9 MeV. The range of these electrons in PMMA is about 4mm so that in this study all incident electrons were stopped by the dielectric.

The electron beam was calibrated by ionization and energy methods, so that irradiation levels are expressed in terms of dose in Grays. Expressed as a charge density, the dose of 3 KGy amounts to about $1\mu\text{C/cm}^2$ of injected electrons. Noise reduced the accuracy at the lowest 10 Gy dose levels to about $\pm 50\%$.

The pulsed electro-acoustic method yields volume charge information by applying a short pulse electric field to the sample and measuring the resultant mechanical pressure wave which arrives at the electrodes [2,3]. The shock magnitude and time delay of arrival are measured with a piezoelectric transducer and provide information about the size and distribution of the volume charge. Figure 2 shows a diagram of this type system.

VIII. Initial Charge vs. Dose

To show the efficiency of the charge trapping process, the net accumulation of charge within the samples at almost constant irradiation time = 30 sec when at room temperature was measured and found to increase linearly with dose (injected charge) up to about 0.1 kGy. At higher doses, a saturation-type response occurs, Figure 3. This may result from one or more of the following processes: charge repulsion by the already trapped volume charge, radiation induced conductivity, and/or heating which reduces relaxation time. Typical mean charge depths were measured to be 2.2mm.

IV. Charge Relaxation vs. Dose

For the various initial charge levels as determined by dose, the decay of net volume charge in samples held at room temperature was measured over a period extending to two months, Figure 4. The samples remained shorted on all sides by wrapping with metal foil during the storage interval between measurements. Two characteristics are readily seen in these curves. First, the relaxation time greatly depends upon dose. For example, whereas the sample irradiated to 3 kGy decays a charge by a factor of 50 in 1,000 hours, the sample irradiated with about 70 Gy showed less than a factor of 2 charge decay in 1,000 hours. Second, all curves appear to extrapolate to a single asymptote of form $1/ct$, where a is a constant $1.6 \times 10^4 (\text{C-hr})^{-1}$ and t is time in hours for the 7cm^2 area.

V. Charge Relaxation vs. Temperature

Additional samples stored at 60°C and 90°C were measured for charge relaxation with the same dose, 3 kGy, as that for the reference room temperature test ($\approx 28^\circ\text{C}$). In addition, a sample at dry ice temperature, -80°C , was irradiated to 1.5 kGy. The resultant decay curves are shown in Figure 5. Solid lines are drawn with a shift by a factor of 10 for each 30°C change in temperature. Note the $1/ct$ asymptotes are shifted by a factor of 10, too. The data at dry ice temperature showed no significant decay even though the total charge of $2\mu\text{C}$ ($0.29\mu\text{C}/\text{cm}^2$) was relatively high.

VI. Charge Relaxation Model

The dependence of charge relaxation time on net volume charge is a phenomena which contradicts traditional constant conductivity models used to describe "resistive" decay with a magnitude independent time constant of ϵ/σ . The charge dependent conductivity data supports a mobility model of the form:

$$\bar{J} = \rho\mu\bar{E} \quad (1)$$

where ρ is the volume charge density, μ is the carrier mobility, and \bar{E} is the electric field. Continuity and Poisson's equation for a single carrier species yields:

$$0 = \frac{\partial \rho}{\partial t} + \frac{\mu}{\epsilon} \rho^2 + \mu\bar{E} \cdot \nabla \rho \quad (2)$$

For a small gradient in charge density, the solution is:

$$\rho = \frac{\rho_0}{1 + \frac{\mu\rho_0}{\epsilon} t} = \rho_0 \frac{\tau}{t + \tau} \quad (3)$$

where ρ_0 is the initial charge density and τ is the relaxation time:

$$\tau = \frac{\epsilon}{\mu\rho_0} \quad (4)$$

which depends upon ρ_0 . For the simple case of a uniform ρ_0 and single dominant carrier, integration over the thickness yields:

$$\frac{q}{q_0} = \frac{1}{a q_0 t + 1} \quad (5)$$

where q is the initial charge per unit area and a is a constant:

$$a = \frac{\mu}{\epsilon d} (\text{coul-sec})^{-1} \quad (6)$$

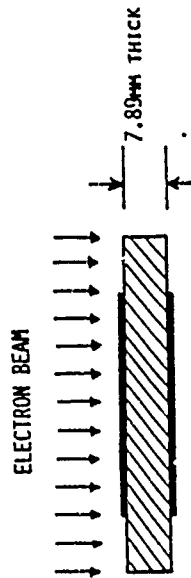


FIGURE 1. SAMPLE GEOMETRY, 5CM X 5CM WIDTH, 7.89MM THICK, 30MM DIA. METALLIZATION

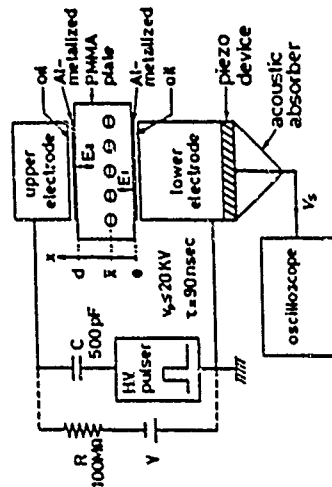


FIGURE 2. PULSED ELECTRO-ACOUSTIC MEASUREMENT SYSTEM

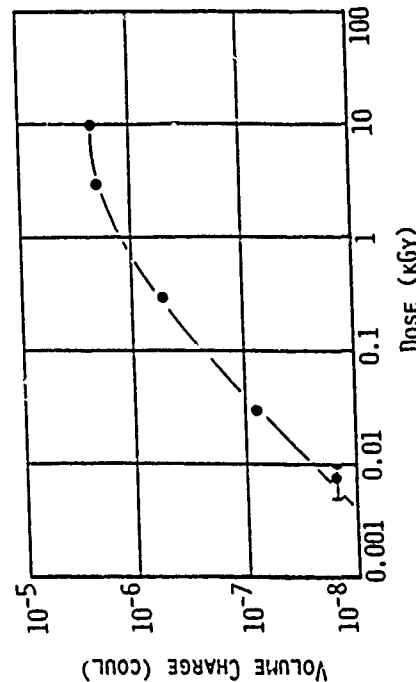


FIGURE 3. INITIAL TRAPPED CHARGE FROM 1 MEV ELECTRONS IN PMMA

The equation for charge relaxation, Eq. (5), is plotted in Figure 6 and appears to be consistent with the low dose data of Figure 4. At higher doses, accelerated charge relaxation, perhaps associated with radiation induced conductivity or multiple carriers appears to dominate initially, and after about 1,000 hours the self-relaxation at constant mobility is seen.

The thermal effects may be modelled as a thermally dependent mobility, where:

$$\mu = AT^3 e^{-Vg/kT} \quad (7)$$

with T in degrees absolute and A and Vg constants. For a factor of 10 change in mobility with a 30°K change near room temperature, Vg has a value of about 0.83eV. Hence, from the room temperature data, $\mu = 8.4 \times 10^{-16} \text{ m}^2/\text{v-sec}$. And with the temperature effect included:

$$\mu = 8.2 \times 10^{-9} T^{-1} e^{-Vg/kT} \quad (8)$$

Further measurements will be needed to evaluate this low dose and low dose rate mobility model and to adjust it to allow for charge transport at the higher dosages.

References

- [1] C.W. Mangelisdrorf and C.M. Cooke, "Bulk Charging of Epoxy Insulation Under DC Stress," Conf. Record of 1980 IEEE Internat. Symp. on Electrical Insulation, 146-149, June 1980.
- [2] T. Takada, T. Maeno, and H. Kushibe, "An Electric Stress Pulse Technique for the Measurement of Charges in a Plastic Plate Irradiated by an Electron Beam," Proc. 5th IEEE Internat. Symp. Electrets, 450-455, Heidelberg, Germany, 1985.
- [3] T. Maeno, H. Kushibe, T. Takada, and C.M. Cooke, "Pulsed Electro-acoustic Method for the Measurement of Volume Charges in E-Beam Irradiated PMMA," 1985 Annual Report Conf. on Electrical Insulation and Dielectric Phenomena, 389-397.

ELECTRIC FIELD INDUCED GAS EMISSION FROM PVDF-FILMS

E. Bihler, K. Holdik and W. Eisenmenger
Physikalisches Institut Teil 1, University of Stuttgart
Pfaffenwaldring 57, 7000 Stuttgart 80, FRG

1. Introduction

The conduction mechanism in insulating polymers can be studied by means of pressure and temperature dependence of electric current $I(t)$. Pressure dependent measurement of the conductivity in the piezoelectric polymer PVDF (poly(vinylidene fluoride)) indicates ionic charge transport. An activation volume of $25 \dots 100 \text{ \AA}^3$ of the ionic charges was found $/2/$.

The direct identification of ionic charge carriers can be obtained by studying the emission of gas atoms from polymers under electric field. For Nylon 66 films a corresponding H_2 emission has been observed $/3/$.

A similar but more sensitive method with discrimination of the polarity influence is used in the present paper to gain information about ionic charge transport in PVDF. The charge transport is an important process during formation (polarization) of piezoelectric PVDF films $/4/$.

2. Experimental

Polymer films of a thickness of $25 \dots 50 \text{ \mu m}$ were installed in an UHV-system with built-in quadrupole mass spectrometer for residual gas analysis.

The films were covered on one side with evaporated copper electrodes (thickness 150 nm , area 20 cm^2), on the other side a copper wire gauze (width of the meshes approx 90 \mu m) was used as a permeable electrode which faces towards the mass spectrometer. A detection of changes in the residual gas composition with a sensitivity of $2 \cdot 10^{-8}$ mbar according to $5 \cdot 10^{-12} \text{ A}$ is possible.

In order to reduce saturation influences on the gas emission by charge accumulation at the electrode-sample interface the electric field ranging from 0 to 1 MV/cm was applied in almost triangular pulse form of a few 100 ms duration. Fig. 1 shows the applied voltage pulse (a) and the gas emission response (b) of H^- ions at the negatively poled electrode. We expect that primarily

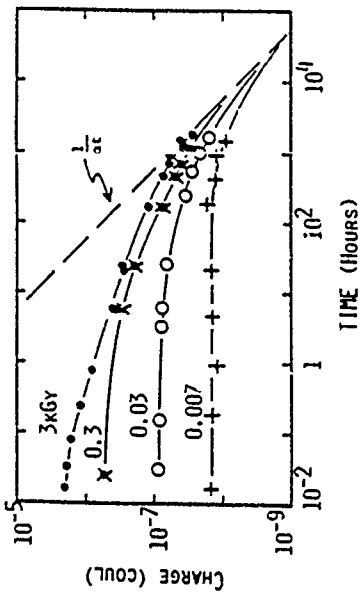


FIGURE 4. CHARGE RELAXATION IN PMMA AFTER IRRADIATION AT 1 MeV

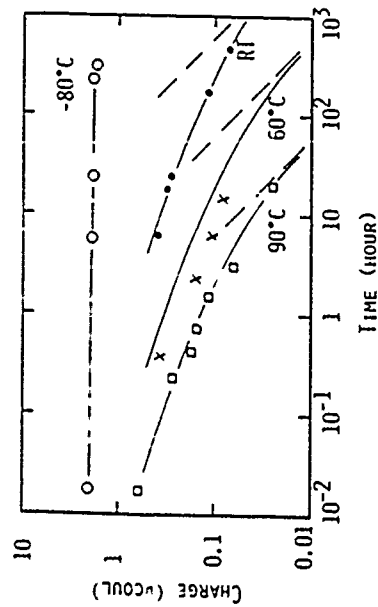


FIGURE 5. TEMPERATURE EFFECT ON CHARGE RELAXATION

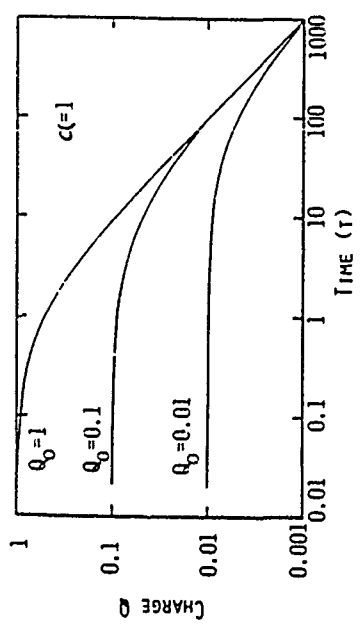


FIGURE 6. CALCULATED CONSTANT MOBILITY CHARGE RELAXATION

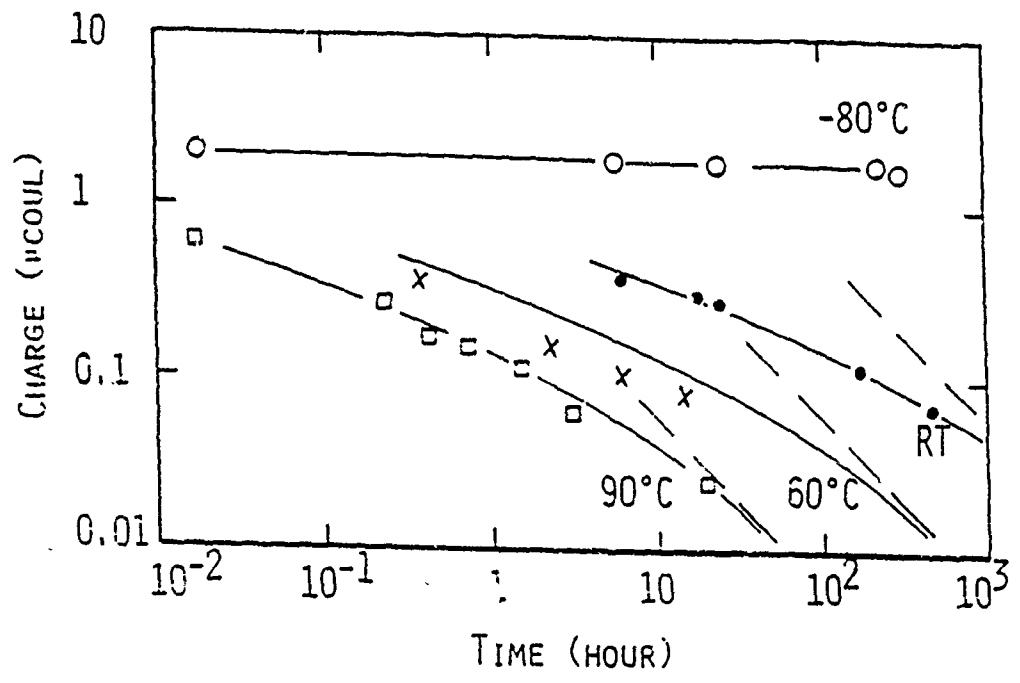


Figure 24 Temperature Effects on Charge Relaxation

MIT-HURL

30°C change in temperature. Note the $1/3t$ asymptotes are shifted by a factor of 10, too. The data at dry ice temperature showed no significant decay even though the total charge of $2 \mu\text{C}$ ($0.29 \mu\text{C}/\text{cm}^2$) was relatively high.

4.1.3 Mobility model

The dependence of charge relaxation time on net volume charge is a phenomena which contradicts traditional constant conductivity models used to describe "resistive" decay with a magnitude independent time constant of ϵ/σ . The charge dependent conductivity data supports a mobility model of the form:

$$\bar{J} = \rho\mu\bar{E}$$

where ρ is the volume charge density, μ is the carrier mobility, and E is the electric field. Continuity and Poisson's equation for a single carrier species yields:

$$\frac{\partial \rho}{\partial t} + \frac{\mu}{\epsilon} \rho^2 + \mu\bar{E} \cdot \nabla \rho = 0$$

For a small gradient in charge density, the solution is:

$$\rho = \frac{\rho_0}{1 + \frac{\mu\rho_0 t}{\epsilon}} = \rho_0 \frac{\tau}{t + \tau}$$

where ρ_0 is the initial charge density and τ is the relaxation time:

$$\tau = \frac{\epsilon}{\mu\rho_0}$$

which depends upon ρ_0 . For the simple case of a uniform ρ_0 and a single dominant carrier, integration over the thickness yields:

$$\frac{q}{q_0} = \frac{1}{1 + \frac{t}{\tau}} \quad (1)$$

where q_0 is the initial charge per unit area and α is a constant:

$$\alpha = \frac{\mu}{\epsilon D} \quad (\text{coul-sec})^{-1}$$

The equation for charge relaxation, Eq. (1), is plotted in Figure 25 and appears to be consistent with the low implanted charge data of Figure 20. At higher implanted charge levels, accelerated charge relaxation, perhaps associated with radiation induced conductivity or multiple carrier species appears to dominate initially, and after about 1,000 hours the self relaxation at constant mobility is seen.

The thermal effects may be modelled as a thermally dependent mobility, where:

$$\mu = AT^3 e^{-(V_g/kT)}$$

with T in degrees absolute and A and V_g constants. For a factor of 10 change in mobility with a 30°C change near room temperature, V_g has a value of about 0.88 eV. Hence, from the room temperature data, $\mu = 8.4 \times 10^{-16} \text{ m}^2/\text{v-sec}$. And with the temperature effect included:

$$\mu = 8.2 \times 10^{-9} T^3 e^{-V_g/kT}$$

Further investigation of this model could be made especially with consideration of varying the rate of implanting charge. Also adjustments for the case of high total injected charge could be studied.

4.2 Initial Net Internal Volume Charge

To show the efficiency of the charge trapping process, the net accumulation of charge within the samples at almost constant irradiation time = 30 sec, when at room temperature, was measured and found to increase linearly with beam charge (injected charge) up to about 0.1 kGy. At higher beam charges, a saturation-type response occurs, see Figure 20. This may result from one or more of the following processes: charge repulsion by the already trapped volume charge, radianon induced conductivity, and/or heating which reduces relaxation time.

4.3 Position of Charge Layer

Typical mean charge depths were measured for several e-beam implantation energies. The results show that the mean charge position is at a depth somewhat greater than the channel position but less than the electron range in the material, see Figure 4. This value is consistent with e-beam stopping calculations published in the literature.[10]

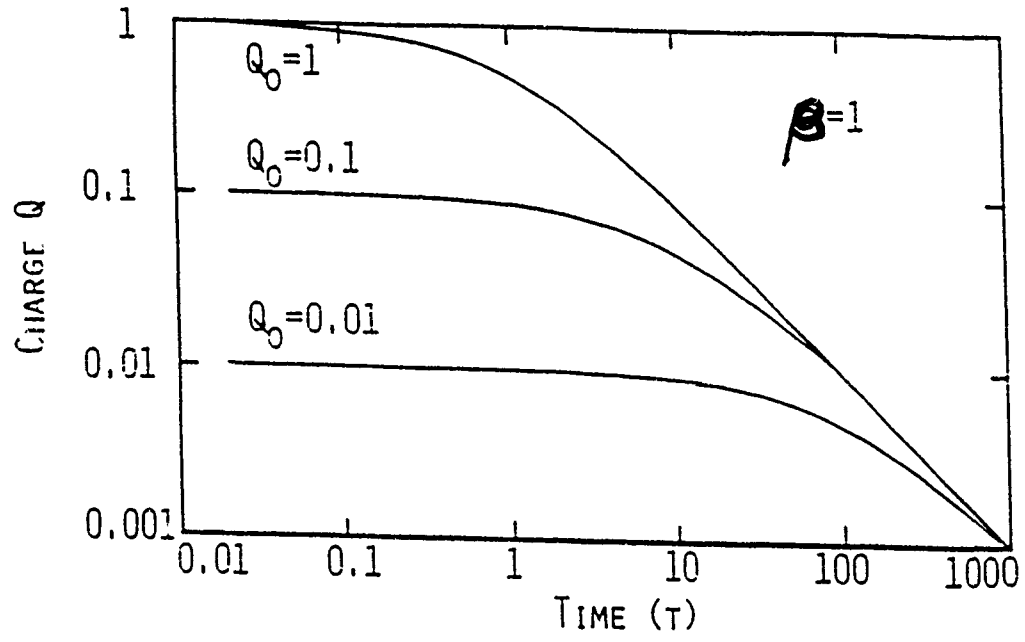


Figure 25 Calculated Constant Mobility Charge Relaxation

MIT-HURL

5. MODEL FOR BREAKDOWN THROUGH VOLUME SPACE-CHARGED REGIONS

5.1 Propagation Model

5.1.1 Absolute available energy

Because there is no applied electric field from an external power supply, the discharges investigated in these studies demonstrate very clearly that energy to propagate a breakdown event can come from static charges distributed in a volume. How the discharge propagates can be interpreted as based upon electric fields and the forces they exert on charge carriers or as electrostatic energy which is converted to light and heat as the system lowers its overall internal energy.

In the field driven model, a discharge propagates when the field resulting from the trapped charges exceeds a threshold field value, E_{th} , necessary to compensate for loss processes. For the self-breakdown case, space-charges and their images at surfaces are the sole source of the field. This means, for a uniform initial charge, that the internal field depends linearly on charge density. For a uniform layer of thickness w , remaining length H , charge density ρ_0 , as depicted in Figure 26, The space charge field, E_s , at the edge is:

$$E_s = \frac{\rho_0 w}{\pi \epsilon} \left\{ \frac{H}{w} \operatorname{arccotg} \left(\frac{2H}{w} \right) - \frac{z}{w} \operatorname{arccotg} \left(\frac{2z}{w} \right) \right. \\ \left. + \frac{1}{4} \ln \left[\left(\frac{1}{4} + \left(\frac{H}{w} \right)^2 \right) \right] - \frac{1}{4} \ln \left[\left(\frac{1}{4} + \left(\frac{z}{w} \right)^2 \right) \right] \right. \\ \left. - \frac{1}{4} \ln \left[\frac{(L+z)^2 + d^2}{z^2 + d^2} \right] \right\}$$

thus :

$$E_s = k_s \rho_0.$$

In this model the channeling should continue as long as charge was available. To account for the experimental finding of self-stopping of channels in materials such as PMMA, Section 3.1.2, it is necessary to have a means by which less field is available at the propagating front of the discharge. Two mechanisms for this have been identified, and they are discussed further in the next section (5.1.2).

For the energy model, it is assumed that the power to sustain the discharge and its losses [5,6] is derived from the change in electrostatic energy before and after the breakdown channeling has past through a region times the velocity of propagation.

$$P_z = \Delta U_s(z) \times v_f(z)$$

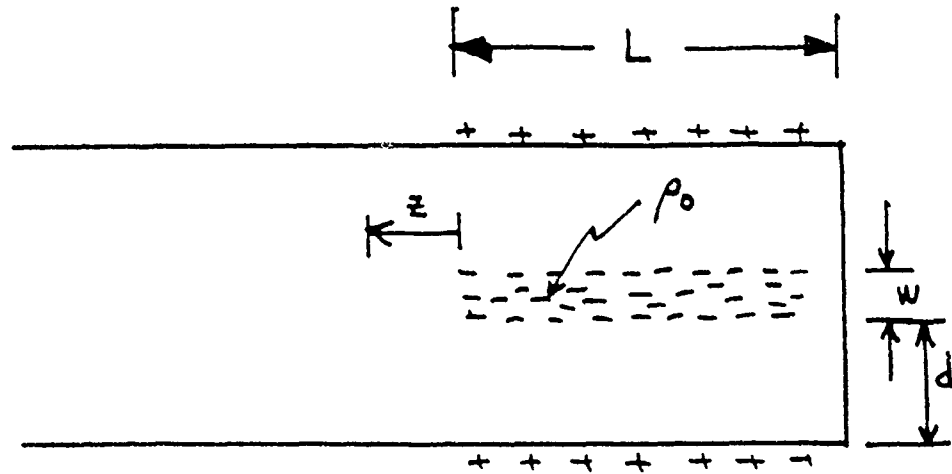


Figure 26 Geometry for Edge Field Calculation

MIT-HURL

where P_z is the power needed per unit propagation in the z-direction, $U_s(z)$ is the electrostatic energy per unit distance in the z-direction, and v_f is the propagation front velocity.

Hence a principle question is the amount of energy available. To determine this, the electrostatic energy associated with an implanted charge and the energy after a channel front has propagated through the charge is determined so as to evaluate the change in energy. To obtain a value for the energy after a discharge has occurred, a model for the channeling was used. It assumes a conducting plane at potential, ϕ_c , taken to be zero; ie. the channel impedance is zero. A conducting plane is used as an equivalent for the discharge which is actually composed of many closely space channels.

A calculation for the change in electrostatic energy by the discharge was made assuming a geometry similar to the experiments. A dielectric sheet of material of thickness $2R_0$, is used where the distance, R_0 , is the maximum penetration distance of the charge layer. The charge is actually located mainly in a layer of finite thickness, but for the calculation the charge is assumed to be distributed in one of two forms: constant or linearly increasing with depth, both to a maximum depth of R_0 . The configurations and results are shown in Figures 27 & 28. For both it is seen that the energy change for discharge channels at a depth a from the surface, is sharply at a maximum for specific positions of the discharge, $x=a/R_0$. Specifically, it is seen that energetically the discharge will strongly prefer to be at a depth of about 0.7 times R_0 . This value is in close agreement with the experimental findings. The equations for the initial energy, U_0 , and the change in energy, ΔU , are for the case of uniform charge density to R_0 :

$$U_0 = \frac{\rho_c^2 R_0^3}{24\epsilon} \left(1 + \frac{3}{2}\right)$$

and

$$\Delta U = \frac{\rho_c R_0^3}{24\epsilon} \frac{5}{2} - \left[x^2 + (1-x^2) \left(1 + \frac{3}{2-x}\right) \right]$$

While for the case of linearly increasing charge density, these values are:

$$U_0 = \frac{\rho_c^2 R_0^5}{6\epsilon^2} \left(\frac{2}{5} - \frac{1}{6}\right)$$

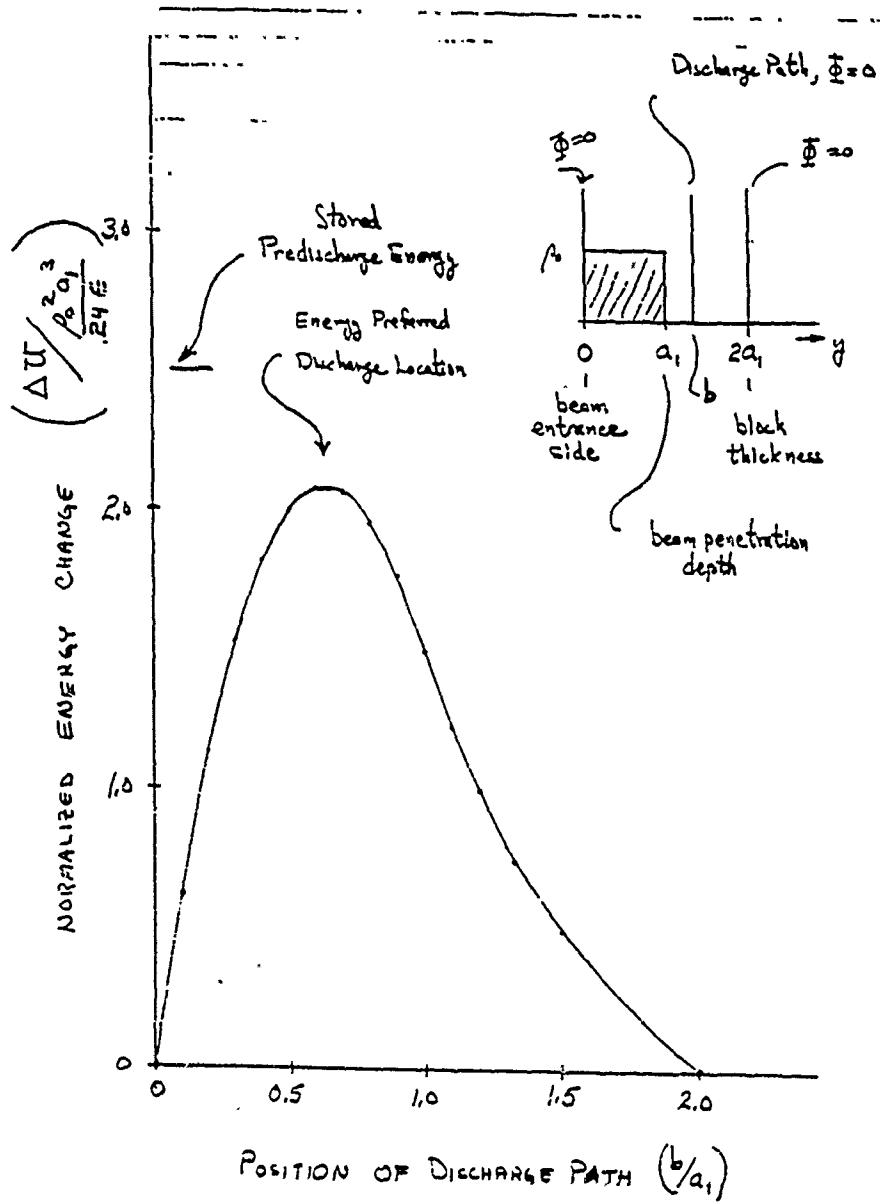


Figure 27 Calculated Energy Preferred Discharge Channel Location, Uniform Charge to a Depth Equal to the Range, in a Material of Thickness 2 times the Range

MIT-HURL

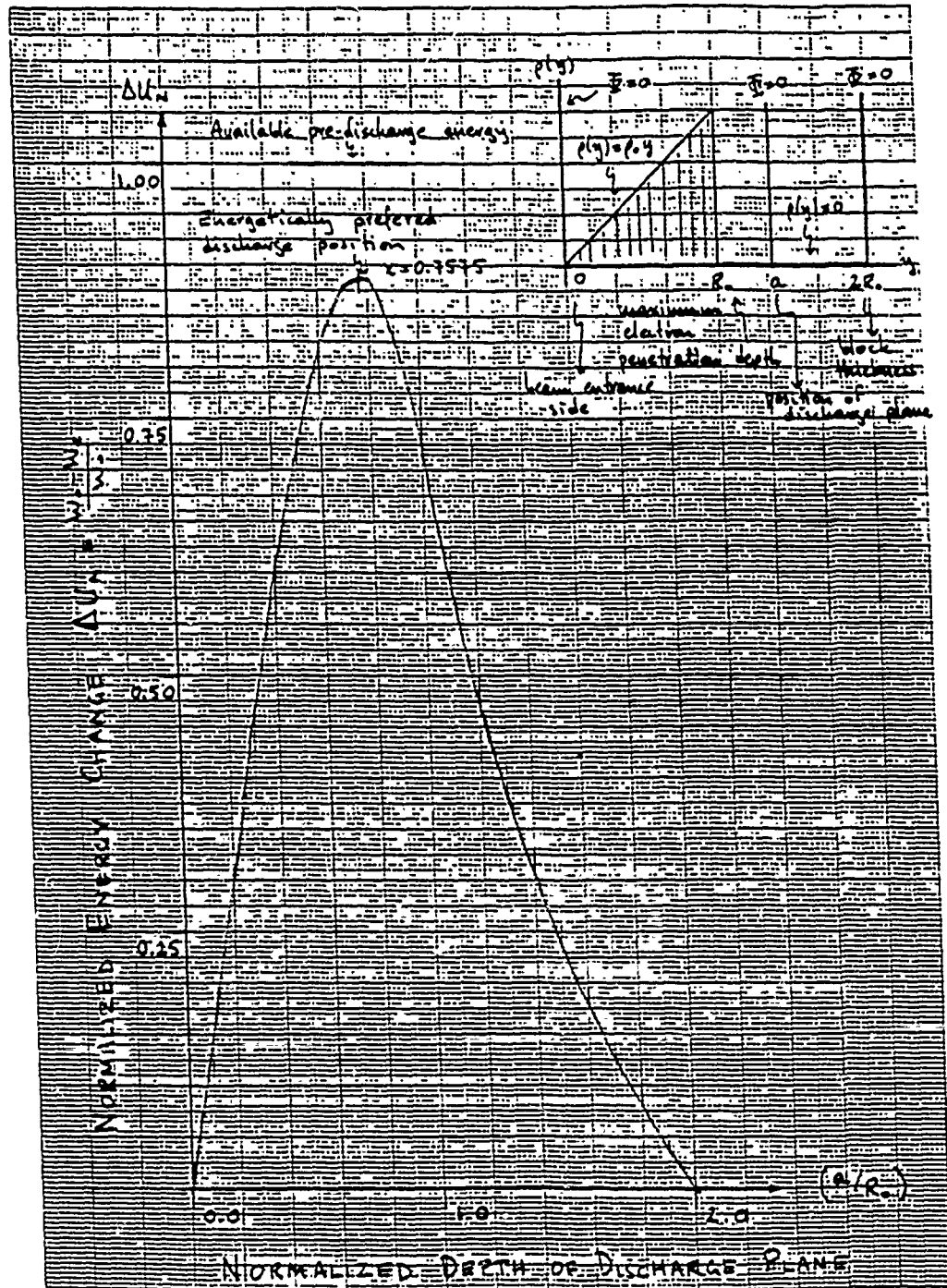


Figure 28 Calculated Energy Preferred Discharge Channel Location, Linearly Increasing Charge Density to a Depth Equal to the Range in a Material of Thickness 2 times the Range

$$\Delta U = \frac{7\rho_0^2 R_0^5}{180 \epsilon^2} \left[1 - \frac{15}{7(2-x)} \left(\frac{x^5}{3} - \frac{4x^3}{3} + \frac{9x}{5} - \frac{14}{15} \right) \right]$$

5.1.2 Relative available energy, Channel impedance effects

While the above model describes the depth of the channeling, it is necessary to account for the self-stopping length. If the efficiency of charge neutralization by the discharge channels is not unity, then a remanant charge remains and there is a lower field at the propagating discharge front. But another way to model self-stopping effects is to allow a finite impedance to the discharge channels so that there is a voltage drop along the length of the channels.

Using a one-dimensional model, the tip potential, ϕ_f , will differ from the ground potential, 0, at the beginning root of the discharge. It will increase with channel length according to the integral of voltage drop per unit length of channel, E_c , over the length of the channel.

$$\phi_f = - \int_0^L E_c(l,t) dt$$

Expected values for E_c , according to the literature, [5,6] indicate that:

$$E_c \approx k_c j^{1/2}$$

where j is the channel current density. Expressed in another way the channel resistance per unit length varies inversely with the square root of current density. Now letting the channel propagation velocity be proportional to the available energy per unit length of travel, we have that velocity is initially proportional to the charge density squared. This is because

$$\Delta U = K [\rho_0^2]$$

As the channel becomes long, the finite resistance lowers the tip potential, lessening the energy per unit path available, this lowers the channel current density at the channel tip. But, because it was shown by the variable implanted charge density studies that the whole length of channel quickly responds to changes at the tip, the whole channel will also have a reduced current density.

Now this provides rapid feedback to cause even greater tip potentials and hence lower energy available because the lower current density raises the channel resistance and thereby raises the voltage drop. This progressive reduction in channeling rapidly comes to a complete halt when the available energy per unit length of growth drops below the threshold power needed to sustain the channel development. Another factor which may occur is a change in the needed power to sustain a

a channel due to its ablation of the material which expands the channel diameter.

Thus, channel propagation is modelled as being driven by the available energy associated with the channel developing into a charged region exceeding the power expended for that development. Furthermore, to explain the experimental findings of well defined self-stopping lengths for some materials, a finite, current dependent resistance of the channels is employed.

5.2 Proposed Model for Charge Injection and Breakdown without E-beam

A fundamental long-term failure process in solid dielectrics often occurs as an internal branched channel structure, which because of its shape is referred to as an 'electrical tree'. This tree channeling usually develops over a period of time at stress with the channel branches progressively extending until one or more in series bridge the distance between the electrodes. The failure is observed as electrical conduction via a connecting path through one or more of the interconnecting channels. Cables bushings, capacitors and other high voltage apparatus can fail because of the treeing process.

The extension of existing branches and the development of new branches in an electrical tree results in the tree 'growth' or expansion. This growth is proposed, based upon the results of these investigations, to occur as a three-step process which is composed of:

- 1) charge injection and accumulation
- 2) discharge initiation
- 3) discharge propagation

The first, injection and accumulation, is dependent upon insulator material, electrodes, applied electric stress and temperature. The second, initiation, is dependent upon the magnitude of the first stage and on the applied stress. while the third, propagation, is relatively independent of temperature and the type of initiation. The three steps normally repeat rapidly so as to yield an almost continuous looking tree growth over a period of time. Alternately, the growth may exhibit distinguishable steps with an apparent pause between steps associated with the time for charge accumulation and initiation.

As an example of electrical treeing and a comparison with channel discharges created by e-beam implanted charge, Figure 29 shows side views for trees originating from high field point electrodes. A pointed electrode brought adjacent a small beam charged region is used for comparison.

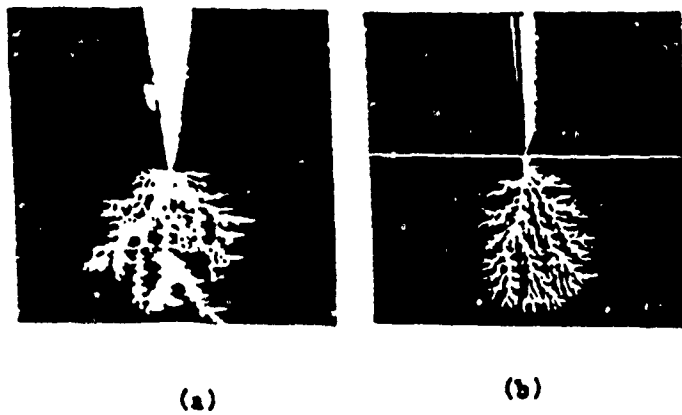


Figure 29 Electrical Discharge Channels in PMMA, (a) AC Voltage with 3mm Point-to-Plane Gap, (b) e-beam Implanted

MIT-HVRL

6. NEW DIAGNOSTICS

Two methods of measurement of implanted charges in solid dielectrics were used to evaluate the charge magnitude and distribution. One employed the Kerr electro-optic effect, ie. birefringence, while the other employed a new electro-acoustic method. Both are described below.

6.1 Electro-optic Measurements of e-beam Implanted Charges

The electro-optic method yields volume charge information by applying incident light polarized preferably 45° to the direction of the internal electric fields in the sample. After passing through the sample, the light is passed through a second polarizer at 90° to the first. This configuration is depicted in Figure 30. [7] The resultant transmitted light intensity is modulated by the internal field so that by examining the fringe pattern a complete mapping of the internal fields is obtained. Some difficulty was encountered with the mechanical birefringence which introduced an initial fringe pattern. Simple thermal annealing did not remove these mechanical stresses so that it was necessary to subtract their effects by assuming that they remained constant. Monochromatic green light from a mercury discharge lamp was used to remove the light wavelength dependence of the birefringence.

Typical results are shown in the photographs of Figure 31 where a portion of the sample surface was irradiated. The changing patterns during the decay period after irradiation is stopped, clearly show the initial field and its relaxation as the charges leave, Figure 32, in addition to the initial mechanical stress. The dark and light regions of the fringe pattern, min and max, show the field exceeds a MV/cm.[7] The line of zero field, ie. the potential maximum, lies below the surface as does the charge max at the fringe density maximum, in correspondence to the discharge channeling depth.

6.2 Electro-acoustic Method

The electro-acoustic method was developed by Prof. Takada from Musashi Institute of Technology in Japan. [8] He came to MIT for a technical visit and collaborated in making test measurements for this study on samples implanted with electrons by the MIT accelerator.

The method yields volume charge information by applying a short pulse, typically about 90 ns, electric field to the sample and measuring the resultant mechanical pressure wave which arrives at the electrodes [8,9]. The shock magnitude and time delay of arrival are measured with a piezoelectric transducer and provide information about the size and distribution of the volume charge. Figure 33 shows a schematic of the system. A typical acoustic pressure waveform for an e-beam irradiated sample shows the three pulses two for the surface image charges and one for the implanted charge peak in the volume, Figure 34. Two publications about this method have been made and are attached.

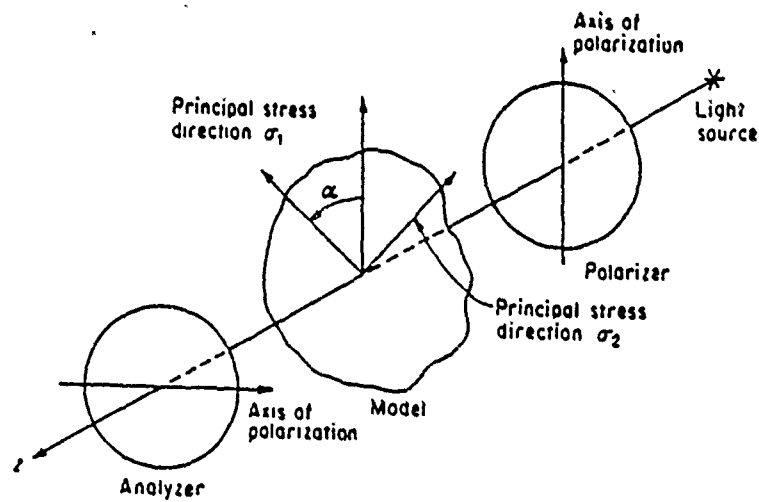


Figure 13.3 A stressed photoelastic model in a plane polariscope.

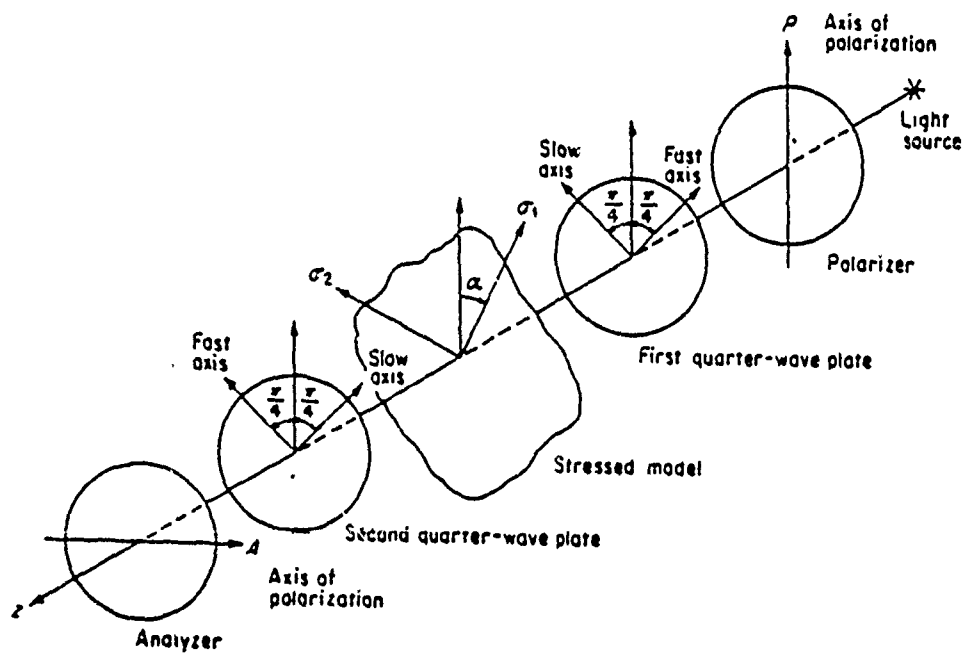
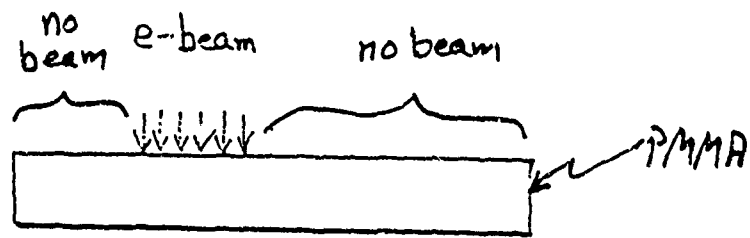


Figure 13.7 A stressed photoelastic model in a circular polariscope (arrangement A, crossed polarizer and analyzer, crossed quarter-wave plates).

Figure 30 Electro-Optic Method of Internal Charge Measurement
(from Optical Methods)



e-beam irradiation: 150 krad, 2.5 MeV
1 inch wide strip

E-O Image after 15 min



E-O Image after 1 hr

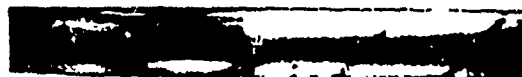
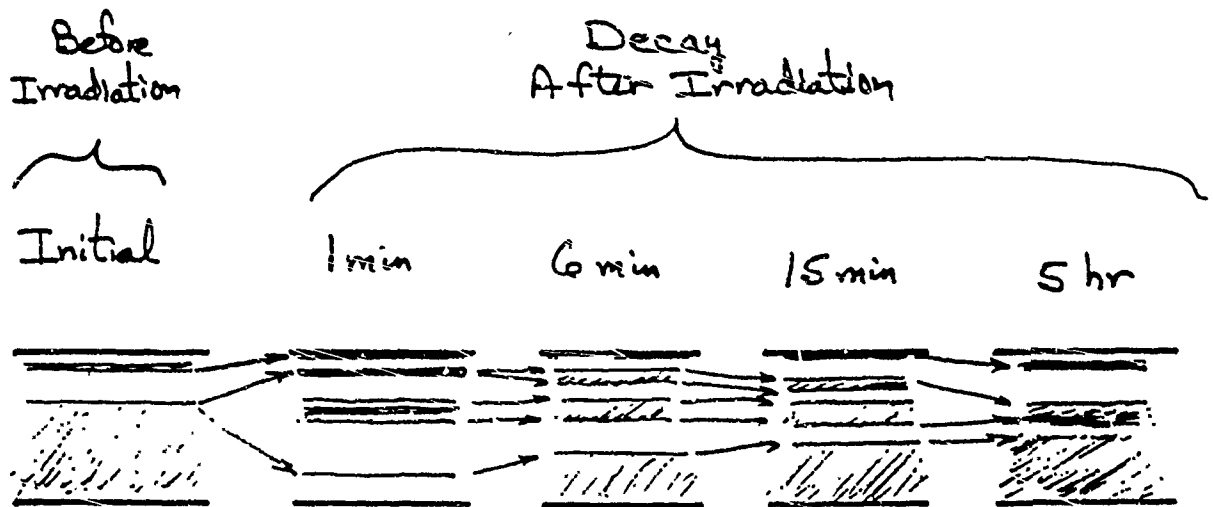


Figure 31 Localized Irradiation of PMMA Sample, 12.7mm Thick
and 10cm Long Optical Path Showing Fringe Shift

MLT-HVAL
CMC



Irradiation: 200 krad , 2.5 MeV electrons

Material: PMMA, 2.5 cm thick, 9.6 cm long path

Figure 32 E-beam Implanted Charge Decay in PMMA, Visualized by Optical Method

MIT-HURL
CMC

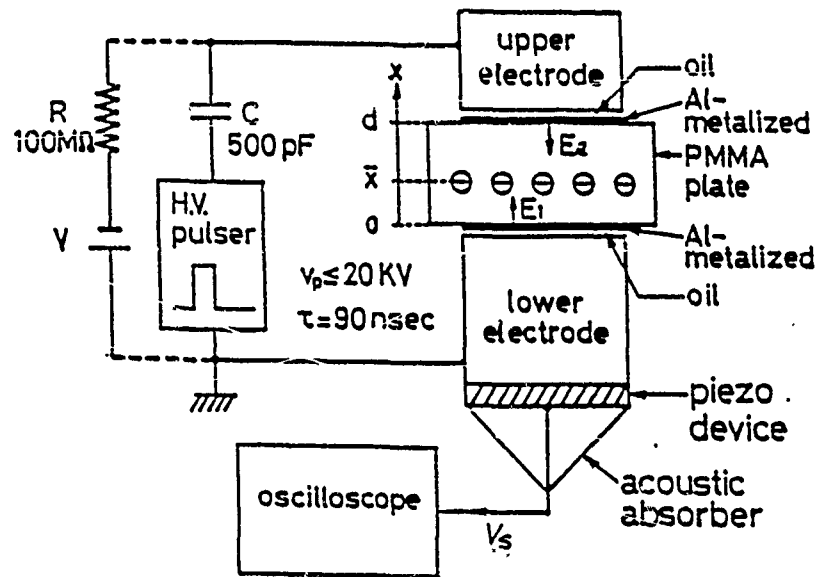


Figure 33 Pulsed Electro-Acoustic Method Measurement System

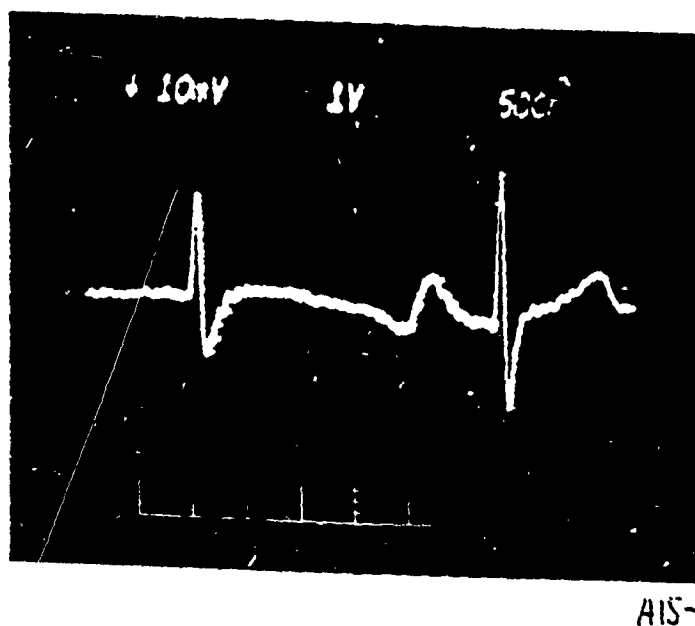


Figure 34 Waveform from Pulse Electro-Acoustic Charge Detection System

PMMA 7.8 mm Thick

1 MeV e-beam

1.2 $\mu\text{C}/\text{cm}^2$ injected

MIT-HURL

7. CONCLUSIONS

The investigations were successful and yielded new information about fundamental physical processes responsible for major limitations in the performance of electrical insulation, especially for high stress applications such as used in pulse power and space satellites. New models to account for charge accumulation in the volume of dielectrics were developed. The accumulation of large internal charges by the e-beam irradiation at a depth below the surface was substantiated by four independent means; visible discharge channels, electro-optics, electro-acoustics, and calculation: Figures 4, 31, 34, and 27,28, respectively. The discharge process was studied in detail and a three stage breakdown model was formulated. The role of available prompt energy to discharge channel development was investigated by means of the unique charge implantation method. This clearly demonstrated that static space charges can be the source of electrostatic energy which drive a discharge. Different materials were investigated to show major parameters which were common and those which were different. The development of dark, carbonaceous looking channels was found to correspond to lower channeling resistance materials. The acoustic and optic space charge probing methods are new diagnostics which were employed in this study and are an additional benefit of the program.

8. ACKNOWLEDGEMENTS

This project benefitted from initial studies in the area of electron beam induced space charged regions and discharges through them. These initial studies were supported by NSF, and were concerned with producing laboratory scale test arrangements for lightning discharge research. Many of the e-beam charging techniques were developed under NSF support and that support is gratefully acknowledged.

The research and discussions about the results were greatly aided by Dr. Earle Williams, then a postdoctoral fellow at MIT and now Associate Professor. Electron beam handling and technology was under the guidance of Kenneth Wright, radiation physicist at the laboratory. His continued attention to the problems in this work made it possible to achieve many of the test results.

9. REFERENCES

- 1] Cooke, C.M., E.R.Williams and K.A.Wright, "Electrical discharge propagation in space charged PMMA", Proc. IEEE Int'l Symp. on Electrical Insulation, Phil, PA, p.95 (1982).
- 2] Gross, B. and K.A.Wright, "Charge Distribution and Range Effects Produced by 3 MeV Electrons in Plexiglas and Aluminum", Phys. Rev. 114, 715 (1959).

- 3] Tong, D.W., "Space Charge probing with an Electron Beam", IEEE Intn'l Symp. on Elect. Insulation, Boston, MA, June (1980).
- 4] Mandelbrot, B.B., The Fractal Geometry of Nature, W.H.Freeman and Co. N.Y.
- 5] Neimeyer, L., "Evaporation-dominated High-Current Arcs in Narrow Channels", IEEE Trans. PAS-97, 950 (1978).
- 6] Wheeler, C.B., "The High Power Constricted Plasma Discharge Column Theory" J.Phys D. 3, 1374 (1970).
- 7] Kim, K.S., T.C.Cheng and D.E.Cooper, "Kerr Effect In Solid Polymethylmethacrylate and Polyethylene", J. Appl. Phys. 54(1), 449 (1983).
- 8] Takada, T., T. Meano and H. Kushibe, " An Electric Stress Pulse Terchnique for the Measurement of Charges in a Plastic Plate Irradiated by an Electron Beam", IEEE Intn'l. Symp. on Electrets, 450, Heidelberg, Germany (1985).
- 9] Maeno, T., H. Kushibe, T. Takada and C.M.Cooke, "Pulsed Electro-Acoustic Method for the Measurement of Volume Charges in E-Beam Irradiated PMMA", Ann. Rept. on Elect. Insul. and Dielectric Phenomena, Buff, NY, 389 (1985).
- 10] Tanaka, R. etal, "The Effect of Accumulated Charge on Depth Dose Profile in PMMA Irradiated with Fast Electrons", IEEE Trans Nucl Sci. 26 4670 (1979).

10. RELATED PUBLICATIONS LIST

- Cooke, C.M., E.R.Williams, and K.A.Wright, "Electrical Discharge Propagation in Space-Charged PMMA" Proc. IEEE Intn'l Symp on Elect. Insulation, Phil., PA, 95 (1982).
- Williams, E.R., C.M.Cooke and K.A.Wright, " Electrical Discharge Propagation in and Around Space Charge Clouds", J. Geophys Res. 90, 6059 (1985).
- Cooke, C.M., E.R.Williams and K.A.Wright, "Space Charge STimulate Growth of Electrical Trees", Proc. IEEE Intn'l. Conf. on Prop. and Applic. of Dielect. Mat'ls, Xian, China June 1985.
- Maeno, T., H. Kushibe, T. Takada and C.M.Cooke, "Pulsed Electro-Acoustic Method for the Measurement of Volume Charges in E-Beam Irradiated PMMA", Ann. Rept CEIDP, NY, 389 (1985).